Atmospheric Environment 167 (2017) 625–641

Contents lists available at ScienceDirect

Atmospheric Environment

journal homepage: www.elsevier.com/locate/atmosenv

Characteristics of size-resolved atmospheric inorganic and carbonaceous aerosols in urban Shanghai

X.X. Ding, L.D. Kong*, C.T. Du, A. Zhanzakova, H.B. Fu, X.F. Tang, L. Wang, X. Yang, J.M. Chen**, T.T. Cheng

Shanghai Key Laboratory of Atmospheric Particle Pollution and Prevention, Institute of Atmospheric Sciences, Department of Environmental Science & Engineering, Fudan University, Shanghai, 200433, China

HIGHLIGHTS

- Atmospheric ultrafine and fine particle pollution in Shanghai were very serious.
- Air pollution had close links with NO_3^- and NH_4^+ in condensation and droplet mode.
- Great contribution of SOC in droplet mode to OC and PM pollution.
- Possible connections between the formation of SOC and SNA were revealed by PSCF.

GRAPHICAL ABSTRACT

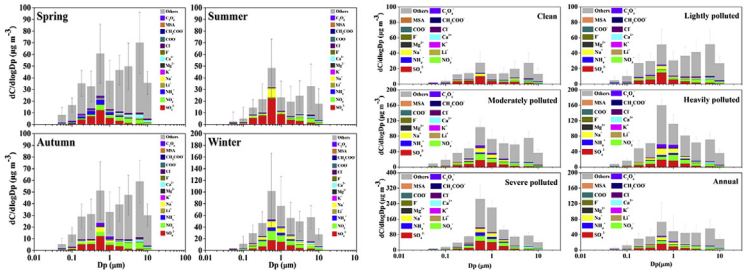

ARTICLE INFO

Article history:
Received 21 March 2017
Received in revised form
12 August 2017
Accepted 17 August 2017
Available online 18 August 2017

Keywords:
Aerosol
Size distribution
Water-soluble ions
Seasonal variation
OC/EC
PSCF

ABSTRACT

Size-segregated aerosol particles were collected with a 10-stage Micro-Orifice Uniform Deposit Impactor (MOUDI) at an urban site in Shanghai, China for four non-consecutive months representing four seasons from 2015 to 2016. Chemical composition, including water-soluble ions as well as organic carbon (OC), elemental carbon (EC) and secondary organic carbon (SOC) of size-resolved (0.056–18 μm) atmospheric aerosols in four seasons and in different polluted cases were studied. The size distributions of sulfate, nitrate and ammonium (SNA) and carbonaceous aerosol (OC, EC and SOC) were discussed and the potential sources of $PM_{1.8}$-associated secondary species (SO_4^{2-}, NO_3^-, SNA and SOC) in different seasons were identified by potential source contribution function (PSCF) model. Results showed that atmospheric ultrafine and fine particle pollution in Shanghai were very serious during the study period. Most of the water-soluble ions tended to be enriched in fine particles, especially being abundant in the droplet mode in polluted cases. Compared with sulfate, size distributions of nitrate and ammonium presented more significant seasonal variations and showed distinctive characteristics in polluted days. Abundant nitrate was concentrated in fine particles in cold seasons (spring and winter), whereas it was enriched in coarse mode during summer and autumn. The droplet mode sulfate with high concentration did not result in the aggravation of air pollution, while the nucleation mode sulfate may have made a great contribution to the air pollution in urban Shanghai. It was also found that the formation of air pollution in urban Shanghai had a significant link with nitrate and ammonium, especially with nitrate and ammonium in condensation mode and droplet mode, and the contribution of sulfate to the pollution formation in Shanghai would somehow be surpassed by the increasing nitrate and ammonium. OC and EC concentrations from spring to winter were found to be 11.10, 7.10, 12.30, 20.16, and 3.73, 2.84, 4.63, 7.10 μg m^{-3},

* Corresponding author.
** Corresponding author.
E-mail addresses: ldkong@fudan.edu.cn (L.D. Kong), jmchen@fudan.edu.cn (J.M. Chen).

http://dx.doi.org/10.1016/j.atmosenv.2017.08.043

respectively, distinctly presenting the summer minima and winter maxima in this study. The maximum OC/EC was in the droplet mode and the minimum was in the nucleation mode for both clean and polluted days. The great contribution of SOC to OC in droplet mode and the occurrence of PM pollution necessarily had an important bearing on the SOC formation in droplet mode particles. Particle acidity may play a key role in secondary organic aerosol formation and the particles with the size of 0.056 −0.1 μm was the most sensitive particles to acid catalysis in SOA formation. The similar PSCF results of $PM_{1.8}$-associated SOC to those of SO_4^{2-}, NO_3^- and SNA indicated possible connections between the formation of SOC and secondary inorganic species in PM.

1. Introduction

As a typical mega-city located in the Yangtze River Delta, Shanghai has experienced an eruption of vehicle population and a sharp increase in energy consumption during the past few decades, which lead to the increasing occurrence of regional air pollution. Air pollution, especially particulate matter (PM) pollution, has drawn increasingly extensive attention in recent years due to its impacts on visibility (Chen and Xie, 2013), human health (Iii et al., 2002; Sheppard et al., 1999; Bell et al., 2006; Underwood, 2017) and climate change (Cifuentes et al., 2001; Forster and Taylor, 2006; Li et al., 2017; Xing et al., 2016). The radiative properties of aerosol are determined by its chemical composition such as sulfate, nitrate, ammonium, mineral dust, soot, organic carbon (OC) and elemental carbon (EC) (Andreae et al., 2008; Laskin et al., 2010), resulting in the decrease of visibility and frequent occurrence of atmospheric pollution events. As secondary aerosols and carbonaceous aerosols in particulate matter have been shown to play a significant role in the atmosphere regarding solar radiation transfer, human health effects, and atmospheric chemistry (Stockwell et al., 2003; Höller et al., 2002; Bond, 2004), studying the chemical composition and the characteristics of PM and its impacting factors is important for air pollution control as well as regional air quality improvement. The size distributions of ambient aerosols provide detailed information on mode distributions and give evidence on the formation and transformation of particulate pollutants in the atmosphere (Whitby, 1978; Hering and Friedlander, 1982; John et al., 1990; Ondov and Wexler, 1998). While several studies have been carried out to investigate the PM chemical species in Shanghai (Wang et al., 2016; Yao et al., 2002; Zhao et al., 2015), few studies on the characteristics of size-resolved atmospheric inorganic and carbonaceous aerosols in different seasons and different polluted conditions in urban Shanghai have been reported.

To better understand air pollution formation, a study linking regional PM chemical characteristics with its size distribution and other influencing factors was imperative. Therefore, a 4-months monitoring program, which started from April 2015 to January 2016, was performed in Shanghai. We measured the concentrations of size-resolved PM and the composition including water-soluble ions (F^-, Cl^-, SO_4^{2-}, NO_3^-, Li^+, Na^+, NH_4^+, K^+, Ca^{2+}, Mg^{2+}, formate, acetate, methanesulfonic acid, oxalate) as well as carbonaceous species (OC, EC and SOC) in clean and polluted days. The correlations between particle sizes, pollutants, meteorology and pollution levels were investigated. The potential sources of $PM_{1.8}$-associated secondary species (SO_4^{2-}, NO_3^-, SNA ($SO_4^{2-}+NO_3^-+NH_4^+$) and SOC) in different seasons were identified by potential source contribution function (PSCF) model. Thus, the characteristics of size-resolved atmospheric inorganic and carbonaceous aerosols in urban Shanghai were further demonstrated. Nowadays China is facing severe particulate pollution, this study will provide useful information on the size-resolved PM pollution in China.

2. Measurements and methodology

2.1. Particle sampling

Size-segregated aerosol samples were collected on the campus of Fudan University (31.30°N, 121.50°E), Shanghai, China (Fig. 1), which is representative of urban Shanghai. The sampling was conducted for 68 days and covered four periods: April (2015), August (2015), October (2015), January (2016), representing spring, summer, autumn, and winter of Shanghai, respectively. Temperature (T), wind speed (WS) and direction, relative humidity (RH) and visibility were routinely measured.

Daily 24-h size-segregated samples in the range of 0.056–18 μm were collected on 47 mm quartz filters (PALLFLEX, USA) using a ten-stage micro-orifice uniform deposit impactor (MOUDI, MSP Corp., USA; Model 110-R) operating at a flow rate of 30 L/min. The equivalent aerodynamic cut-off diameter (Dp) of each stage is 18, 10, 5.6, 3.2, 1.8, 1.0, 0.56, 0.32, 0.18, 0.10, and 0.056 μm, respectively. The particle modes were divided by the cut points and were defined as follows: 0–0.1 μm for nucleation mode, 0.1–0.56 μm for condensation mode, 0.56–1.8 μm for droplet mode, and 1.8–18 μm for coarse mode, respectively. Since the cut point of 2.5 μm is not available in this study, the classification of the polluted cases was based on $PM_{1.8}$ concentrations.

The quartz fiber filters (PALLFLEX, USA) were pre-combusted at 500 °C for 4 h in a muffle furnace to remove original organic traces. The filters were weighed before and after sampling by an intelligent weighing system (Hangzhou Wmade Intelligent Technology co., LTD, reading precision 10 μg) after at least 24 h of equilibration at (20 ± 1) °C and a relative humidity of (40 ± 1) %. The samples and field blank filters were then placed in membrane filter boxes and reserved in a refrigerator under −18 °C prior to analysis. The sampling was taken only when the meteorological conditions were favourable (i.e. no wet precipitation). All of the procedures were strictly quality controlled to avoid any possible contamination of the samples. Eventually, 805 size-segregated aerosol samples were successfully collected and used.

In addition, since the ten aerosol particle size bins of the deposit impactor exhibit an approximately normal distribution against the particle diameter on a logarithmic scale (Marple et al., 1991), dC/$d\log_{10}$Dp (where C is mass concentration and Dp is aerodynamic diameter) was calculated to represent the size resolved concentrations in this study.

2.2. Chemical analysis

One fourth of each aerosol sample and the blank filter were extracted ultrasonically by 5 ml ultra-pure deionized distilled water (specific resistance ≥18.2 MΩ, Millipore) for 40 min. Water extracts of samples and blank filters were analysed for F^-, Cl^-, SO_4^{2-}, NO_3^-, PO_4^{3-}, Li^+, Na^+, NH_4^+, K^+, Ca^{2+}, Mg^{2+}, formate, acetate,

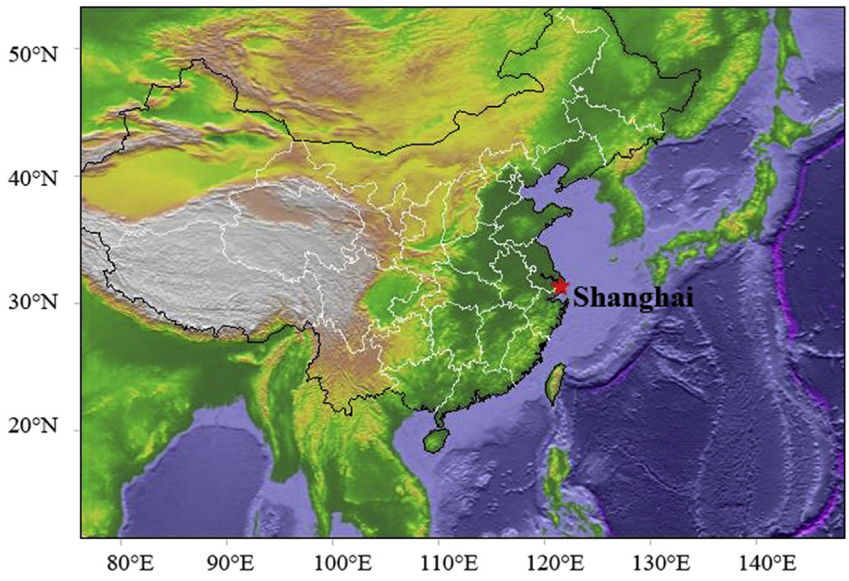

Fig. 1. Location of Shanghai in China.

methanesulfonic acid, and oxalate by ion chromatography (940 Professional IC, Metrohm, Switzerland.) with a separation column of Metrosep A supp 16–250, a Metrosep A supp 16 guard column for anion and a Metrosep C6 analytical column, a Metrosep C4 guard column for cation. The relative standard deviation of each ion was less than 2% from reproducibility tests. OC and EC were determined by a DRI Model 2001 Thermal/Optical carbon analyser (Atmoslytic Inc., Calabasas, CA, USA). A 0.506 cm^2 punch of each sample was analysed for eight carbon fractions following the IMPROVE thermal/optical reflectance (TOR) protocol (Chow et al., 1993). Four OC fractions (OC1, OC2, OC3, and OC4 at 120 °C, 250 °C, 450 °C, and 550 °C, respectively, in a helium atmosphere), three EC fractions (EC1, EC2, and EC3 at 550 °C, 700 °C, and 800 °C, respectively, in a 2% oxygen/98% helium atmosphere) and OP (a pyrolyzed carbon fraction determined by transmittance) were produced. IMPROVE OC is operationally defined as OC1 + OC2 + OC3 + OC4 + OP and EC is defined as EC1 + EC2 + EC3 − OP. The concentrations of OC and EC reported in this study were all corrected for the field blanks.

2.3. Estimates of secondary organic carbon (SOC)

To quantify the contributions of both primary organic carbon (POC) and SOC to carbonaceous aerosol, SOC were evaluated by the minimum OC/EC ratio method in this study. EC has often been used as a tracer of POC for it is mainly emitted from combustion sources and the chemical transformations of EC are limited (Huntzicker et al., 1982; Turpin and Huntzicker, 1991; Gray et al., 1986). In contrast, OC is resulted from both primary emission sources and secondary transformation from primary gaseous organic compounds in the atmosphere (Turpin and Huntzicker, 1995). Thus, an underlying hypothesis was proposed that because EC and primary OC often have the same sources, a representative ratio of primary OC/EC for a given area can exist. If the measured ambient OC/EC ratio exceeds this expected value, then the additional OC is considered to be secondary. Based on this hypothesis, the minimum OC/EC ratio method to estimate the SOC has been proposed. The equation is as follows:

$$OC_{pri} = EC \times (OC/EC)_{pri} \quad (1)$$

$$OC_{sec} = OC_{tot} - OC_{pri} \quad (2)$$

where OC_{pri} is estimated POC, OC_{sec} is estimated SOC, OC_{tot} is measured total OC, EC is measured elemental carbon, and $(OC/EC)_{pri}$ is the ratio of OC to EC in the primary aerosol.

This method has been widely applied because it is simple and alternative, and the required data can be easily obtained or estimated. However, it is difficult to determine the $(OC/EC)_{pri}$ comprehensively for a given area because it is source dependent and is influenced by meteorological conditions. Castro et al. (1999). suggested that $(OC/EC)_{pri}$ could be replaced by $(OC/EC)_{min}$ (the minimum ratio of OC/EC), and thus the equation could be written as below:

$$OC_{sec} = OC_{tot} - EC \times (OC/EC)_{min} \quad (3)$$

The minimum ratio of OC/EC may be affected by many factors such as meteorological conditions, the variation of the emission source, and the migration of aerosols. Thus, SOC concentration derived by the EC tracer method could be significantly underestimated in this study. In order to reduce the influence of contingency to the maximum extent, the $(OC/EC)_{pri}$ we used is the annual minimum of each sampling size.

2.4. pH calculation

Since an established analytical method that directly determines aerosol pH does not exist, thermodynamic modelling approach E-AIM (Extended Aerosol Inorganics Model, http://www.aim.env.uea.ac.uk/aim/aim.php) (Clegg et al., 1998; Wexler and Clegg, 2002; Friese and Ebel, 2010) was employed to explore the characteristics of acidity of size-resolved PM. The E-AIM can be used to simulate gas-aerosol partitioning processes and calculate the equilibrium composition of the aqueous or solid aerosol phase. The aqueous and solid phase of ionic composition in the mixing system $H^+ - NH_4^+ - SO_4^{2-} - NO_3^- - Cl^- - Na^+ - H_2O$ can be accurately

simulated at a given temperature (T) and relative humidity (RH) by E-AIM 4. The T, RH, and molar concentrations of total aerosol acidity ($[H^+]_{Total}$), SO_4^{2-}, NO_3^-, Cl^-, NH_4^+, and Na^+ were used as the input in model 4 of E-AIM to obtain the concentrations of free ions in the aqueous phase, and/or any salt of these ions that was formed in the solid phase at equilibrium. At the same time, the mole fraction and activity coefficient of each ion in aqueous phase were reported. The $[H^+]_{Total}$ was estimated from the ionic balance of the relevant ionic species (Pathak et al., 2008; Zhang et al., 2007):

$$[H^+]_{Total} = 2 \times SO_4^{2-}/96 + NO_3^-/62 + Cl^-/35.5 - NH_4^+/18 - Na^+/23 \quad (4)$$

where SO_4^{2-}, NO_3^-, Cl^-, NH_4^+ and Na^+ in Eq. (4) represent the mass concentrations of ions. Based on model outputs, the in situ particle pH was calculated as follow:

$$pH = -\log(\gamma \times [H^+]_{Frac}) \quad (5)$$

where γ and $[H^+]_{Frac}$ are the activity coefficient on mole fraction basis and the molar fraction of aqueous phase H^+, respectively. While $\gamma \times [H^+]_{Frac}$ represents the aqueous phase activity of H^+. (Zhang et al., 2007).

2.5. Back trajectory analysis and PSCF

48-h backward trajectories of air masses arriving at the sampling site were calculated using the HYSPLIT model (http://ready.arl.noaa.gov/HYSPLIT.php) to investigate the influence of different air masses from distant sources on aerosol composition. The meteorological data fields used to run the model are available at NOAA's ARL archives. Potential source contribution function (PSCF) model was used to identify the likely locations of the sources based on the HYSPLIT model. The zone of concern was divided into $i \times j$ small equal grid cells. All of the hourly endpoints in the back trajectories generated by the HYSPLIT model were classified into $0.2^\circ \times 0.2^\circ$ grid cells. The PSCF values for the grid cells in the study domain were calculated by counting the trajectory segment endpoints that terminated within each cell (Ashbaugh et al., 1985). The number of endpoints that fell in the ijth cell was designated n_{ij} and the number of endpoints for the same cell having arrival times at the sampling site corresponding to PM concentrations higher than an arbitrarily set criterion was defined to be m_{ij}.

The PSCF value for the ijth cell was defined as

$$PSCF_{ij} = m_{ij}/n_{ij} \quad (6)$$

In this study, the annual mean value of a particular species was treated as the criterion, based on trial and error.

To reduce the effect of small values of nij, the PSCF values were multiplied by an arbitrary weight function Wij to better reflect the uncertainty in the values for these cells (Polissar et al., 1998). The weighting function was defined as below.

$$w_{ij} = \begin{cases} 1.00 & 80 < n_{ij} \\ 0.70 & 20 < n_{ij} \le 80 \\ 0.42 & 10 < n_{ij} \le 20 \\ 0.05 & n_{ij} \le 10 \end{cases} \quad (7)$$

3. Results and discussion

3.1. Levels of size-resolved particulate matter in Shanghai

Due to the continuous changes in source emissions, meteorology, photochemical reactions, planetary boundary layer heights, and regional transport, etc. the PM concentrations showed temporally dynamic variations. PM_{18} ranged from 26.39 to 222.22 μg m^{-3}, with an average of 98.58 μg m^{-3}. $PM_{1.8}$ ranged from 7.18 to 169.91 μg m^{-3} and averaged 55.32 μg m^{-3}. PM_1 ranged from 5.79 to 95.25 μg m^{-3} and averaged 42.70 μg m^{-3}. $PM_{0.1}$ ranged from 0 to 29.63 μg m^{-3} and averaged 6.03 μg m^{-3}. Fig. 2 shows the time series of particle size categories measured at Shanghai throughout the whole field campaign. Among the whole field campaign, urban Shanghai's daily $PM_{1.8}$ level exceeded the second grade national standard of China (75 μg m^{-3}) for $PM_{2.5}$ for 10 days and exceeded the first grade national standard (35 μg m^{-3}) for 45 days. The annual concentration of the $PM_{0.1}$ was 6 times higher than that observed in Taiwan (1.42 μg m^{-3}) (Bamber, 2012), PM_1 was much higher than that measured in urban Shanghai (49.8 μg m^{-3}) in 2013–2014 and Beijing (56.6 μg m^{-3}) in 2011–2012 (Qiao et al., 2015; Sun et al., 2015), and $PM_{1.8}$ was 1.6 and 1.8 times higher than the values of $PM_{2.5}$ that measured in North plain in China during 2005–2010 (53.65 μg m^{-3}) and in urban Shanghai during 2011–2013 (47 μg m^{-3}) (Zhao et al., 2013; Wang et al., 2016), respectively. Compared with those studies, the concentration of PM in Shanghai was extremely high, indicating that the atmospheric ultrafine and fine particle pollution in Shanghai during the study period was very serious.

Distinct PM seasonal variations in Shanghai have been observed. As can be seen from Fig. 2, the concentration of PM (such as PM_1, $PM_{1.8}$, and PM_{18}) in winter was much higher than that in summer, while the concentrations of PM in spring and autumn were similar, showing the order of winter > spring > autumn > summer. However, $PM_{0.1}$ presented different seasonal variation and followed the sequence of spring > summer > autumn > winter. The seasonal characteristics of PM mass concentrations in Shanghai can be explained as the combined effect of meteorological conditions, local emissions, and long-range transport. The PM mass concentrations in summer were remarkable lower than other sampling seasons due to the impact of the higher wind speeds and the transport of clean oceanic air masses experienced during the summer time which tend to favour PM dispersion and result in a drop of PM concentration (shown in Fig. S1 in the Supplement). The typically high values in cold seasons lasted from late autumn till early spring. Dominant north and northwest wind during cold seasons which brought relatively polluted overland air masses, and the substantial increase of local emissions from coal combustion in cold seasons combined with the influence of lower mixing layer height and the frequent occurrence of fog-haze episodes under stagnant weather gave rise to the heavier polluted air in cold seasons in Shanghai (Li et al., 2014).

3.2. Size-resolved atmospheric water-soluble components in aerosols

3.2.1. Chemical composition of size-resolved atmospheric aerosols in four seasons

Water-soluble ions F^-, Cl^-, SO_4^{2-}, NO_3^-, Li^+, Na^+, NH_4^+, K^+, Ca^{2+}, Mg^{2+}, formate, acetate, oxalate and methanesulfonic acid were measured. The water-soluble ions in PM_{18} was 34.02 μg m^{-3} for the annual average, with 27.10, 24.37, 29.63 and 49.04 μg m^{-3} in spring, summer, autumn and winter, respectively, constituting 25%, 39%, 33% and 37% of the mass concentration, respectively. For $PM_{1.8}$, the annual average water-soluble ions concentration was 21.65 μg m^{-3}, with 17.10, 16.77, 19.43 and 29.87 μg m^{-3} in spring, summer, autumn and winter, respectively, constituting 32%, 49%, 37% and 40% of the mass concentration, respectively. For PM_1, the annual average concentration of water-soluble ions was 16.33 μg m^{-3}, with 13.71, 13.79, 15.01 and 20.92 μg m^{-3} in spring, summer, autumn and winter, respectively, constituting 31%, 49%, 36% and 39% of the mass

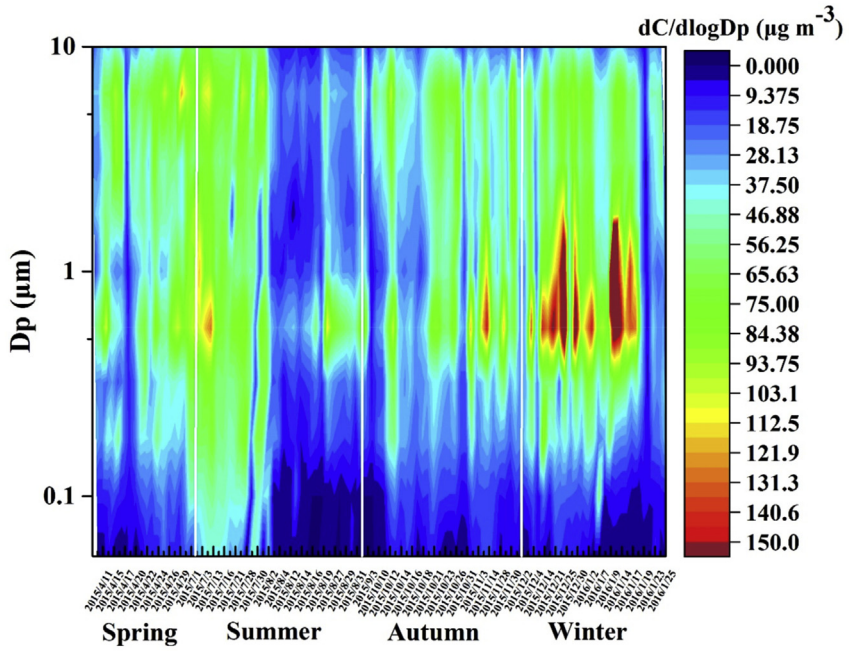

Fig. 2. Time series of particles size categories measured at Shanghai during the whole field campaign from April 10, 2015 to January 26, 2016.

concentration, respectively. While for $PM_{0.1}$, the contribution of water-soluble ions to $PM_{0.1}$ mass concentration was lower than those to PM_{18}, $PM_{1.8}$ or $PM_{1,}$ with the concentrations of 0.90, 1.10, 1.14 and 1.39 μg m^{-3} and with the corresponding fractions of 11%, 18%, 19% and 30% in spring, summer, autumn and winter, respectively. Compared to other seasons, the smallest contribution of water-soluble ions to PM mass in spring was probably related to the long-range transported dust from north and northwest of China, of which a large proportion was water insoluble. In addition, $PM_{0.1}$ usually contains Aitken nuclei (particles with diameters between 10 and 100 nm or so) and fresh aerosols created in situ from the gas phase by nucleation (particles smaller than 10 nm or so). Most of the Aitken nuclei start their atmospheric life as primary particles, and secondary material condenses on them as they are transported through the atmosphere (Seinfeld and Pandis, 2006). Therefore, the high contribution of water-soluble ions to $PM_{0.1}$ mass in winter may be primarily attributed to the condensation of secondary species on primary particles under favourable atmospheric conditions. Mass fractions of water-soluble ions in nucleation mode, condensation mode, droplet mode and coarse mode were 19%, 39%, 49% and 24%, respectively. The mass concentrations of the water-soluble ions followed the sequences of $Cl^- > SO_4^{2-} > Ca^{2+} > NO_3^- > Na^+ > Li^+ > K^+ > NH_4^+ > F^- > Mg^{2+} > C_2O_4^- > CH_3COO^- > HCOO^-$ for nucleation-mode particles, $SO_4^{2-} > NO_3^- > Na^+ > Cl^- > NH_4^+ > Ca^{2+} > C_2O_4^{2-} > Li^+ > K^+ > F^- > Mg^{2+} > HCOO^- > MSA > CH_3COO^-$ for condensation mode, $SO_4^{2-} > NO_3^- > Na^+ > NH_4^+ > C_2O_4^{2-} > Cl^- > Ca^{2+} > K^+ > F^- > Li^+ > Mg^{2+} > MSA > HCOO^- > CH_3COO^-$ for droplet mode, while the sequence was $NO_3^- > SO_4^{2-} > Ca^{2+} > Cl^- > Na^+ > F^- > NH_4^+ > Li^+ > C_2O_4^{2-} > K^+ > Mg^{2+} > CH_3COO^- > HCOO^- > MSA$ for coarse mode particles. Cl^- and Ca^{2+} were the important water-soluble ions and couldn't be ignored in nucleation-mode particles. These results show the concentration characteristics of the different water-soluble ions in different particle size fractions, and may imply a difference in mixing ratios among the dominant chemical compounds involving these ions in different particle modes. The seasonal composition of water-soluble ions in different sizes of atmospheric aerosols were shown in Fig. 3. As shown in Fig. 3, particulate matter presented similar two-peak pattern in four seasons. One peak was in the fine mode (0.56–1 μm), the other in the coarse mode (5.6–10.0 μm). The fine mode was probably mainly attributed to anthropogenic pollutants such as coal burning sources and vehicular emission while the coarse mode was attributed to natural sources, such as mineral dust and sea salt (Han et al., 2005). It should be noted that in spring and autumn, the peak in coarse mode (5.6–10.0 μm) was higher than that in fine mode (0.56–1 μm), while it was just the opposite in summer and winter. The relatively high peak in coarse mode in spring and autumn may be attributed to the impact of the long-range transport originated from northern and northwestern China (Sun et al., 2005). It should be pointed out that a significant portion of PM shown as "Others" in Fig. 3 was observed. The possible composition of the "others" may be insoluble crust materials and metal elements arising from tyre wear, brake wear and resuspension (Zhou et al., 2012; Squizzato et al., 2016), etc. Mineral dust from insoluble crust materials plays complex roles in sulfate and nitrate aerosol formation and new particle formation and growth (Dupart et al., 2012; Liu et al., 2012; Nie et al., 2014; Xie et al., 2015), and hence the composition of the "others" and its potentially roles still needs to be further investigated.

As the dominant pollutants, the secondary inorganic aerosol components (SNA: SO_4^{2-}, NO_3^- and NH_4^+) in PM_{18} were 18.42 μg m^{-3}, 17.49 μg m^{-3}, 14.34 μg m^{-3} and 29.62 μg m^{-3} in spring, summer, autumn and winter, respectively, constituting 17%, 28%, 16% and 24% of the mass concentration, respectively. The ion mass concentrations of SNA followed the sequence of $NO_3^- > SO_4^{2-} > NH_4^+$ in winter while the sequence was $SO_4^{2-} > NO_3^- > NH_4^+$ in other seasons. The sequence of SNA in droplet mode was $SO_4^{2-} > NO_3^- > NH_4^+$ for all the four seasons. For droplet-mode particles, SNA accounting for 33%, 46%, 27% and 31% of the mass concentration in spring, summer, autumn and winter, respectively. The contribution of SNA to the particles in summer was highlighted in the droplet-mode. Thus, the high mass fraction percentage of water-soluble ions in summer that has been mentioned in the earlier discussion was mainly caused by

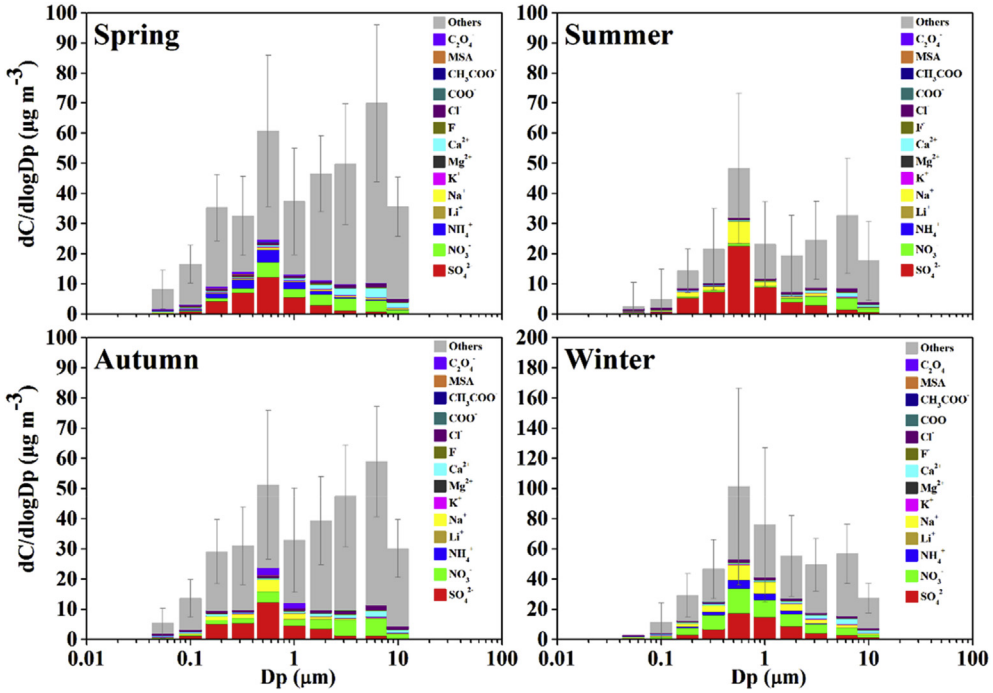

Fig. 3. Size-resolved aerosol composition in four seasons in Shanghai. The marker shows the average mass concentration in each size bin with the error bar representing the standard deviation.

SNA, especially by the SNA in the droplet mode.

The chemical composition of aerosols possessed distinct seasonal variations. Sulfate presented one-peak pattern in four seasons with the peak in the particles with size between 0.56 and 1 μm. The size distribution of sulfate was quite different from a previous study (Whitby, 1978), which characterized the size distribution of sulfate with a trimodal model, consisting of the nucleation mode, the accumulation mode and the coarse mode. Different from other seasons, in summer, sulfate has absolute dominance of SNA concentration. The high contribution of SNA to mass concentration for both PM_{18} and droplet mode particles in summer that has been mentioned above and the high sulfate contribution to SNA did not result in a high particle pollution level for summer (Fig. 2) due to the dominant clean oceanic air sources, showing the characteristics of air pollution in summer. Though the concentration of sulfate in summer was low, its contribution to the mass concentration of SNA was the largest, accounting for 68% of SNA in 0.056–18 μm particles and even 96% of SNA in the droplet mode particles. This shows the dominant contribution of sulfate to SNA and the own characteristics of secondary sulfate pollution in summer in urban Shanghai. Compared with sulfate, the overall concentrations of the nitrate and ammonium presented more significant seasonal variations. Nitrate presented a one-peak pattern in winter, while in other seasons, the log-normal size distribution of nitrate showed a bimodal size distribution with two peaks in the size ranges of 0.32–1 μm and 1.8–10.0 μm. Abundant nitrate was concentrated in fine particles in cold seasons (spring and winter), whereas it was enriched in coarse mode during summer and autumn. In the size range of 0.56–10.0 μm in cold seasons, more nitrate with decreasing size of PM was observed. Ammonium was relatively abundant in spring and winter, with the similar size distribution of nitrate in cold seasons. It accounted for 20% of SNA in PM in spring and the value was reduced to 11% for winter. Moreover, compared to sulfate, ammonium also presented a one-peak pattern in four seasons with the peak in the size range of 0.56–1 μm though less ammonium was observed in summer and autumn. The average temperature decreased from above 28 °C in summer to 9 °C in winter and RH decreased from 70% in summer to 55% in spring, indicating that the variations of NO_3^- and NH_4^+ might be strongly related to the meteorological factors. Due to the thermodynamic instability of ammonium nitrate, the lower temperature and RH in winter and spring favour the shift of thermodynamic equilibrium from gaseous nitric acid and ammonia to particulate phase ammonium nitrate, and thus elevated the levels of NO_3^- and NH_4^+ in fine particles, while the higher temperature and RH in summer and autumn might accelerate the decomposition of ammonium nitrate and thus suppressed the nitrate aerosol formation in fine particles (Wang et al., 2012). The results mentioned above show the remarkable seasonal characteristics of secondary aerosol pollution in urban Shanghai.

In this study, CH_3COO^-, $HCOO^-$ and MSA were present in PM in negligible concentrations, though they were possibly underestimated due to the evaporation of these species in acidic particles in the measurements. $C_2O_4^{2-}$ showed a significantly increase in autumn for the droplet mode particles. The concentrations of Na^+ varied with seasons. The concentration peak of Na^+ was in droplet mode in summer, autumn and winter, while less Na^+ was found in spring. Most Na^+ tended to be enriched in fine particles, especially being abundant in the droplet mode, and this tendency was particularly obvious in winter.

In addition, the mass ratio of $[NO_3^-]/[SO_4^{2-}]$ has been widely used as an indicator of the relative contribution of mobile vs. stationary sources of nitrogen and sulfur in the atmosphere (Xiao and Liu, 2004; Arimoto et al., 1996; Yao et al., 2002). High $[NO_3^-]/[SO_4^{2-}]$ mass ratio means that the mobile sources are more important than stationary sources of pollutants (Arimoto et al., 1996), and vice versa. In this study, the SNA pollution in summer in Shanghai featured the lowest $[NO_3^-]/[SO_4^{2-}]$ mass ratio of 0.22, with relatively high ratios for spring (0.64), autumn (0.68) and winter (1.16). The lowest $[NO_3^-]/[SO_4^{2-}]$ mass ratio found in summer indicates the

absolute predominance of stationary source of pollutants in summer. While the higher $[NO_3^-]/[SO_4^{2-}]$ mass ratios in the spring, autumn and winter may be due to the relatively low temperature, which favoured a shift from the gas phase as nitric acid to the particulate phase as ammonium nitrate. Moreover, the higher $[NO_3^-]/[SO_4^{2-}]$ mass ratios found in our study were also associated with the rapid increase of motor vehicles and the reduction of SO_2 emission resulting from the implementation of SO_2 emission control measures in recent years. The contribution of mobile sources becomes important and may be the dominant source of pollutants in urban shanghai, especially in winter, which can be explained by the extremely high traffic load of transportation in China when approaching the time of Chinese New Year. Due to the traffic stress caused by the large floating population in urban Shanghai at that period, the intensive use of vehicles will definitely increase the emission of nitrogen oxides to the atmosphere. The high mass ratio of $[NO_3^-]/[SO_4^{2-}]$ and high mass concentration of SO_4^{2-} in spring and autumn indicated that both stationary and mobile sources were important to PM pollution in urban Shanghai though the air pollution control measures are implemented during the measurement periods.

3.2.2. Chemical composition of size-resolved atmospheric aerosols in different pollution levels

In order to better understand the change of the atmospheric aerosol composition and its particle size distribution, the polluted cases were further divided into five levels in this study. According to the daily $PM_{1.8}$ concentrations, the pollution conditions of each day were segregated into clean cases ($PM_{1.8} < 35$ μg m^{-3}), lightly polluted cases ($35 < PM_{1.8} < 75$ μg m^{-3}), moderately polluted cases ($75 < PM_{1.8} < 115$ μg m^{-3}), heavily polluted cases ($115 < PM_{1.8} < 150$ μg m^{-3}), and severely polluted cases ($PM_{1.8} > 150$ μg m^{-3}). 25 data sets of size-resolved aerosol samples were collected during clean days and 65 data sets were collected during polluted days (45 lightly polluted days, 17 moderately polluted days, 2 heavily polluted days, 1 severely polluted day).

In our study, the coarse modes showed the largest contribution, accounting for 27–59% of PM_{10} mass, followed by the droplet mode and condensation mode in the range of 18–57% and 11–38% of PM_{10}, respectively. This distribution was quite different from that in Hong Kong sub-urban area (droplet mode > condensation mode > coarse mode > nucleation mode) (Gao et al., 2016), where even the highest PM_{10} concentration (80 ± 13 μg m^{-3}) was lower than the average concentration of PM_{10} in this study, indicating that the increasing particle size for PM in higher polluted areas and the difference might be explained by local emissions, meteorological regimes and regional transport in different sampling sites. As the level of air pollution was aggravating, the atmospheric particles' preference for fine particles became more obvious. When the air was clean, 47% of the mass concentration was attributed to $PM_{1.8}$ while the value was increased to 71% when the air was severely polluted. And the contribution of coarse mode to total PM decreased from 0.37 in clean days to 0.31 in polluted days. These results indicated the increase of the particles with reducing sizes in polluted days and may imply new particle formation and growth in polluted days (Xie et al., 2015; Nie et al., 2014).

The concentrations of the total water-soluble ions in PM_{18} were 16.67 μg m^{-3} and 35.07 μg m^{-3}, accounting for 41% and 28% of the mass concentration of PM_{18} in clean and polluted days, respectively. Mass fraction percentage of water-soluble ions in nucleation mode, condensation mode, droplet mode and coarse mode in clean days were 44%, 47%, 51% and 35%, respectively, and were 13%, 30%, 44% and 20% in polluted days, respectively. The average size-resolved aerosol composition under 5 polluted cases during the sampling periods were compared in Fig. 4. As shown in Fig. 4, the chemical composition of aerosols in different polluted cases possessed a large difference. For those species that has been analysed in this study, they tended to be enriched in fine particles, especially being abundant in the droplet mode during the pollution episodes. As shown in Fig. 4, most composition exhibited significantly higher concentrations in droplet mode compared with that in other modes. Particles tended to have a more complex composition as the aggravating of the pollution level. Both the main species of the particles and the size distribution of each component within the period changed with different levels. Less nitrate, formate, acetic acid, oxalate and methanesulfonic acid were observed during the clean days, whereas the content of those components showed a significant increase as the occurrence of pollution episodes. As an excellent indicator for estimating biomass burning emission and tracing carbonaceous aerosol long-range transport in the atmosphere (Dibb et al., 1996; Liu et al., 2000; Duan et al., 2004; Hsu et al., 2009), water-soluble K^+ showed distinct increase with the aggravating of the pollution level, the concentration of which increased from 0.29 μg m^{-3} in clean days to 0.71 μg m^{-3} in severely polluted days. However, the average concentration of K^+ (0.43 μg m^{-3}) in polluted days was relatively low compared with SNA, indicating that no large-scale biomass burning and its corresponding regional transport appeared during the pollution periods and the biomass burning emission was not the dominant factor for the air pollution. The concentration of Na^+ varied with the pollution levels. The concentration peak of Na^+ was 0.56–0.1 μm in clean days, while the range of the peak expanded to 0.1–1.8 μm in polluted days. And the situation can be applied to most of the species. The concentration peaks for droplet-mode particles were relatively sharper in polluted cases comparing with that in clean days, and with a broader size range from 0.56 to 1.8 μm than 0.56–0.1 μm in clean days. This can be related with the accumulation of precursor pollutants during the pollution formation process. Throughout the whole sampling period, the SNA were the most abundant species, accounting for 21% of the mass concentration of PM_{18}. The average mass concentrations of NO_3^-, SO_4^{2-} and NH_4^+ were 8.66, 12.28, 1.58 μg m^{-3} in polluted days, respectively, much higher than those in clean days (2.19, 8.03 and 0.18 μg m^{-3}, respectively). Therefore, the formation of the pollution events in the observation periods were mainly influenced by the secondary aerosol pollution. Although the concentration of SNA (10.70–52.48 μg m^{-3}) increased synchronously with the increase of pollution level, the ratios of SNA/PM (0.20–0.23) did not present significant difference between the five different polluted cases. As can be seen in Fig. 4, less nitrate was observed during the clean days in urban Shanghai, whereas a significant increase of nitrate occurred with the occurrence of pollution episodes. With the increasing of the pollution level, the fraction of nitrate and ammonium in SNA (i.e., $(NH_4^+ + NO_3^-)$/SNA) increased from 0.31 in clean days to 0.42, 0.56, 0.38, 0.65 in lightly polluted days, moderately polluted days, heavily polluted days, severely polluted days respectively, which indicated that the enhanced formation of nitrate and ammonium in polluted days and their increasing contribution to the air pollution in urban Shanghai. SO_4^{2-} was the most abundant species of SNA, accounting for 35–69% of SNA in PM mass, and the value even reached to 72–81% in fine particles. However, its contribution to the pollution formation in Shanghai would somehow be surpassed by the increasing nitrate and ammonium.

3.2.3. Characteristics of size-resolved SNA on polluted days

As mentioned in 3.2.2, controlling the fraction of nitrate and ammonium in SNA will effectively help to reduce the air pollution in urban Shanghai, thus the characteristics of size-resolved SNA will be further discussed in this section. Fig. 5 presented the size

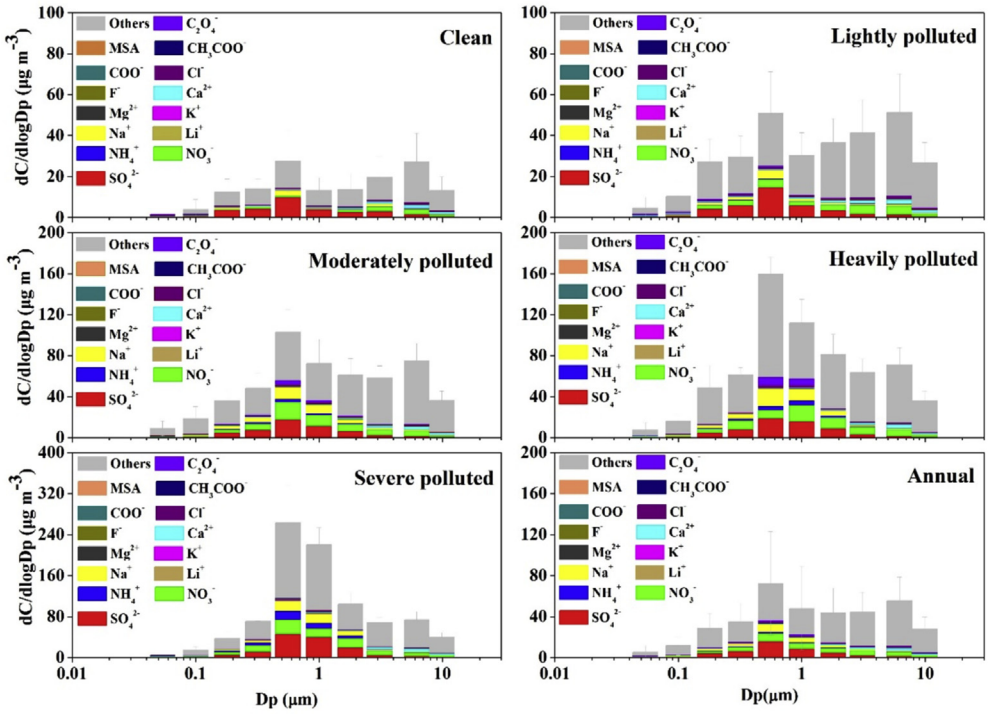

Fig. 4. Size-resolved aerosol composition under 5 polluted cases (**a**. clean, **b**. lightly polluted, **c**. moderately polluted, **d**. heavily polluted, **e**. severely polluted). The marker shows the average mass concentration in each size bin with the error bar representing the standard deviation.

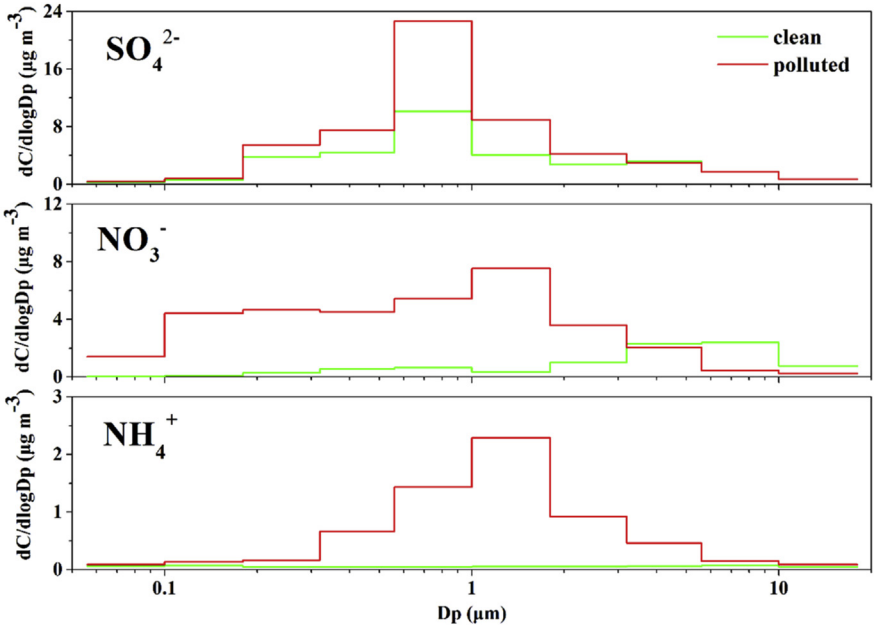

Fig. 5. Log-normal size distributions of sulfate, nitrate and ammonium in clean and polluted conditions.

distribution of sulfate, nitrate and ammonium in clean ($PM_{1.8}$ < 35 μg m^{-3}) and polluted ($PM_{1.8}$ > 35 μg m^{-3}) days. As shown in Fig. 5, sulfate presented one peak mode in both clean and polluted cases with the peak size of 0.56–1 μm. Nitrate and ammonium showed a broad peak from 3.2 to 10 μm in clean days and presented a peak in the particles with size between 1 and 1.8 μm in polluted days. A small peak was also found in 0.18–0.32 μm for nitrate in polluted days. It was notable that the concentration of nitrate in particles of the diameter >3.2 μm was higher in clean days than in polluted days. The sequence of SNA in coarse mode was NO_3^- > SO_4^{2-} > NH_4^+ in polluted days and SO_4^{2-} > NO_3^- > NH_4^+ in clean days, respectively. For fine particles, the sequence of SNA was SO_4^{2-} > NO_3^- > NH_4^+ for both clean and polluted days.

Table 1 compared the chemical components of size-resolved PM in polluted and clean days. As shown in Table 1, the nucleation

Table 1
The ratios of the concentrations of size-resolved components in particulate matter in polluted and clean days during the field observation in Shanghai.

Species	Period	Nucleation mode	Condensation mode	Droplet mode	Coarse mode	PM_{18}
PM	Polluted/Clean	3.88	2.75	3.32	2.57	2.85
SO_4^{2-}		2.2	1.38	1.78	1.11	1.53
NO_3^-		/	7.86	13.77	2.31	3.96
NH_4^+		1	13	35	2.5	8.58
NO_3^-/SO_4^{2-}	Clean	0.24	0.30	0.17	1.40	0.73
	Polluted	0.64	0.53	0.60	1.89	1.13
NH_4^+/SO_4^{2-}	Clean	0.21	0.03	0.01	0.12	0.09
	Polluted	0.20	0.14	0.13	0.12	0.14
$R_{C/A}$	Clean	0.69	0.13	0.04	0.25	0.26
	Polluted	0.52	0.30	0.24	0.19	0.28
pH	Clean	0.64	0.67	0.74	0.66	0.67
	Polluted	0.68	0.84	1.01	0.68	0.77

mode presented the highest ratio of size-resolved PM concentration in polluted and clean days, followed by droplet mode and condensation mode, and the sequence was consistent with sulfate, indicating that though the concentrations of nucleation mode PM and sulfate were less than that of other modes, their influence on the air pollution formation cannot be ignored. Considering that the droplet mode sulfate with high concentration did not result in the aggravation of air pollution (discussed in Section 3.2.1), we speculated that maybe the contribution of sulfate to the air pollution in urban Shanghai was mainly caused by the nucleation mode sulfate, and relatively small shifts of the nucleation mode sulfate can result in substantial differences in the aerosol scattering coefficient and thus result in visibility degradation under appropriate meteorological conditions (Seinfeld and Pandis, 2006; Tao et al., 2015).

Except nitrate in nucleation mode, the concentration of the chemical components presented in Table 1 in each mode increased by 1–35 fold during pollution episodes. Extreme increase of the nitrate and ammonium concentration was observed for particles in condensation mode and droplet mode, indicating that the formation of air pollution in urban Shanghai had a significant link with nitrate and ammonium, especially with the nitrate and ammonium in condensation mode and droplet mode.

As mentioned in Section 3.2.2, the fraction of nitrate and ammonium in SNA (i.e., $(NH_4^+ + NO_3^-)$/SNA increased significantly with the pollution level, while the contribution of sulfate to the pollution formation in Shanghai somehow tend to recede by the influence of nitrate and ammonium, connecting with the extreme augment of the nitrate and ammonium during polluted days in condensation and droplet mode rather than coarse mode particles, we speculated that during the processes of the formation of secondary aerosols in the polluted days, fresh nitrate and ammonium were mainly formed in the fine particles, and with the aging of the aerosols, the conversions of the formed unstable ammonium-containing species including ammonium nitrate might go from fine to coarse particles. The SNA in Shanghai featured high $[NO_3^-]/[SO_4^{2-}]$ mass ratio of 1.13 in polluted days, with relatively low ratios (0.73) for clean days. The increasing $[NO_3^-]/[SO_4^{2-}]$ mass ratio in coarse mode from 1.40 in clean days to 1.89 in polluted days, indicating that the large contribution of mobile source to coarse particle pollutants in urban shanghai. In contrast, the $[NO_3^-]/[SO_4^{2-}]$ ratio was lower than 1 in fine particles in clean and polluted days, which indicates that the stationary emissions were still the dominant source of the fine particle pollution.

3.2.4. Characteristics of acidity of size-resolved PM

The ion balance expressed by the equivalent charge ratios ($R_{C/A}$) of the major cations was usually used to estimate the neutralizing level of atmospheric aerosols (Adams et al., 1999; Zhang et al., 2002; He et al., 2012):

$$R_{C/A} = ([NH_4^+]_{eq} + [Ca^{2+}]_{eq})/([SO_4^{2-}]_{eq} + [NO_3^-]_{eq}) \quad (8)$$

where $[NH_4^+]_{eq}$, $[Ca^{2+}]_{eq}$, $[SO_4^{2-}]_{eq}$ and $[NO_3^-]_{eq}$ stand for the concentrations of their equivalent charges, respectively.

As shown in Table 1, the average equivalent charge ratios for PM_{18} were 0.26 and 0.28 in clean days and polluted days, respectively, both were lower than unity ($R_{C/A} = 1$), indicating that particles in Shanghai were acidic. Compared with the previous studies, the $R_{C/A}$ of our study was significantly lower than those measured in Beijing (0.93 in haze period, 1.10 in clear period) (Wang et al., 2006) and Guangzhou ($R_{C/A} = 2.5$) (Wu et al., 2006), indicating that the aerosol acidity of urban Shanghai was stronger than those areas. Calculated pH of size-resolved PM in polluted and clean days were presented in Table 1. The average pH of size-resolved particles in the clean and polluted days were 0.67 and 0.77, respectively, consistent with the results of $R_{C/A}$, showing that the size-resolved aerosols were acidic during the whole observation period. The pH of condensation mode particles in this study was comparable to PM_1 pH (0.77 ± 0.96) estimated in the northeastern United States in winter (Guo et al., 2016). Fig. 6 presented the size distribution of calculated pH as a function of PM_{18} concentration. As shown in Fig. 6, particles with size between 0.56 and 1 μm all owned the highest pH in different polluted cases. The relationships between secondary organic carbon (SOC) and pH for different size-resolved particles were shown in Table S1. As shown in Table S1, for most size-resolved particles (except particles with the sizes of 0.56–1 μm and 1–1.8 μm), the concentrations of SOC increased with the increasing of the acidity of aerosols, indicating that acid catalysis may play a key role in secondary organic aerosol (SOA) formation (Guo et al., 2016) and the acidity may have implications on pollution levels (Zhao et al., 2015). For particles with the size between 0.056 and 0.56 μm, the correlation coefficients between SOC concentration and pH decreased with the increasing of the particle size, indicating that the acidic condition might lead to more SOA formation for aerosols with smaller diameters (Jang et al., 2002). These results implied that controlling the acidity of the small aerosols (with the size of 0.056–0.1 μm) might be a possible way to reduce the SOA pollution in Shanghai.

3.3. Characteristics of size-resolved carbonaceous aerosols

3.3.1. Size distribution of carbonaceous species in four seasons

Based on the minimum OC/EC ratio method, the size distribution of carbonaceous species (OC, EC and SOC) of particulate matters in four seasons in Shanghai were presented in Fig. 7. As shown in Fig. 7, the average concentrations of carbonaceous species had similar seasonal patterns (winter > autumn > spring > summer) to particulate mass (winter > spring > autumn > summer). OC and EC concentrations from spring to winter were 11.10, 7.10, 12.30, 20.16,

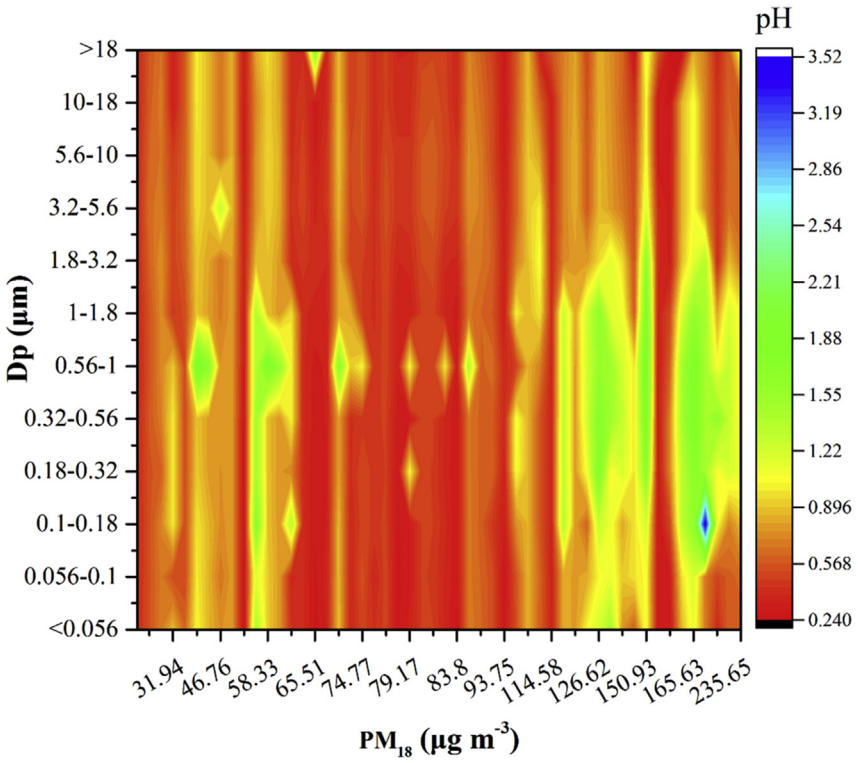

Fig. 6. Calculated pH of size-resolved PM.

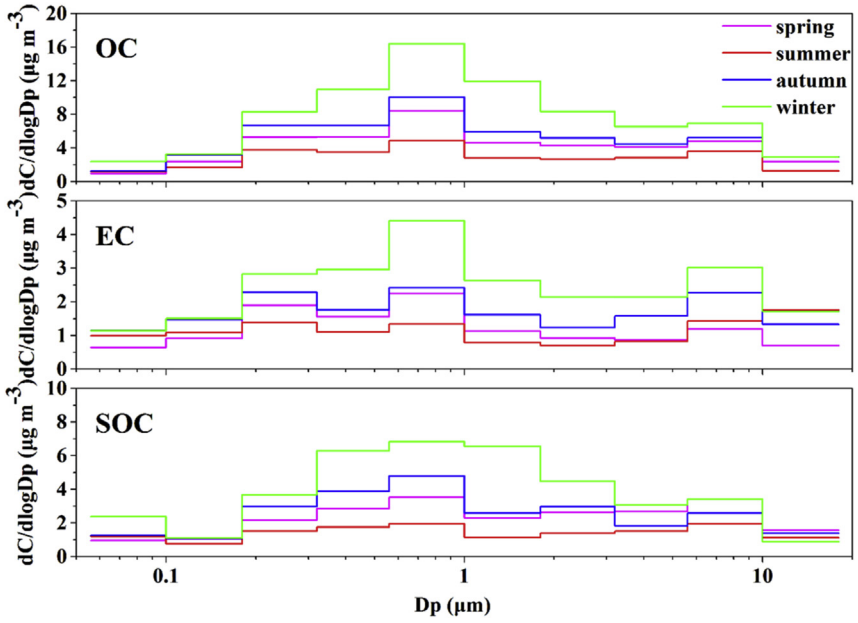

Fig. 7. Log-normal size distributions of carbonaceous species (OC, EC and SOC) of particulate matters in four seasons in Shanghai.

and 3.73, 2.84, 4.63, 7.10 μg m^{-3}, respectively. The levels of OC and EC in fine particles ($PM_{1.8}$) during winter were 3.0 and 1.8 times higher than those in summer and 2.8 and 1.9 times higher for OC and EC in PM_{10}, respectively. The maximum carbonaceous species in $PM_{1.8}$ appeared on January 2, 2016, 16.56 μg m^{-3} for OC and 6.13 μg m^{-3} for EC respectively, sum of which, i.e. total carbon (TC) accounted for about 19.7% of $PM_{1.8}$ (112.85 μg m^{-3}). It was because that increasing source emissions from intensive energy consumption, low mixing height and low precipitation during winter may contribute to the high carbon loading during cold season.

The SOC concentration ranged from 0.855 to 12.04 μg m^{-3}, with the average of 5.63 ± 3.45 μg m^{-3}. SOC averagely accounted for about 56% of the total OC concentration. The SOC concentration and contribution to OC in this study were higher than those reported in other areas, such as Taiwan (4.2 μg m^{-3} and 40%) (Lin and Tai, 2001)

and San Joaquin Valley of California (20%) (Strader et al., 1999). The average SOC concentrations in Shanghai were 6.28, 3.61, 6.95 and 10.36 μg m^{-3} in spring, summer, autumn and winter respectively, accounting for 57%, 51%, 57%, 51% of OC, respectively, indicating the significant role of secondary transformation in carbonaceous pollution in Shanghai. The highest seasonal average SOC observed in winter may be attributed to the increasing emission rate of primary carbonaceous particles and organic gases in winter which were mainly produced by the fuel combustion processes. The stable atmosphere and low temperature in winter facilitated the accumulation of the precursors of SOA (SOA = 1.6 × SOC) (Turpin and Huntzicker, 1995) and accelerated the adsorption and condensation of semi-volatile and intermediate-volatile organic compounds into aerosols (Wang et al., 2016). The low temperature in winter also favoured gas–particle equilibrium to move towards the particulate phase. As a result, the SOA formation was accelerated in winter (Strader et al., 1999). The observed lowest seasonal average SOC concentration in summer and its similar SOC/OC ratio to other seasons may be due to the low levels of organic precursors and OC though the high temperature and strong sunlight in summer favour the photo-chemical secondary transformation.

As shown in Fig. 7, carbonaceous species presented similar two-peak pattern in four seasons. One peak was in the fine mode (0.56–1 μm), the other was in the coarse mode (5.6–10.0 μm). Abundant carbonaceous species were concentrated in fine particles, especially in winter. The concentration peaks for fine particles were relatively sharper in winter, while for OC and EC, there also exist an extra small peak range from 0.18 to 0.32 μm in fine particles in spring, summer and autumn. The size distributions of SOC in four seasons were rather different from OC and EC. While it still presented with two main peaks (0.56–1 μm and 5.6–10.0 μm), it also featured with two small peaks with the size range between 0.056-0.1 μm and 1.8–3.2 μm for fine particles and coarse particles, respectively, indicating the complex transformation mechanism of OC.

Table 2 presented the concentrations of the size-resolved carbonaceous aerosols and the seasonal variations of OC/EC, SOC/OC in different size mode particles during the field observation in Shanghai. The daily average OC and SOC in the whole period followed the sequence of coarse mode > droplet mode > condensation mode > nucleation mode, while the order of EC was coarse mode > condensation mode > droplet mode > nucleation mode. The $PM_{1.8}$-associated carbonaceous aerosols almost contribute half of the total carbonaceous aerosols. For $PM_{1.8}$-associated SOC, it accounted for 50%, 44%, 55% and 51% of $PM_{1.8}$-associated OC in spring, summer, autumn and winter respectively, with seasonal concentrations of 3.47, 2.00, 4.49, 6.94 μg m^{-3}. With the same SOC/OC ratio in PM_{18}, the SOC/OC ratio in $PM_{1.8}$ was higher in autumn than in spring. For nucleation mode, the SOC/OC ratio in summer was quite lower than those in other seasons, indicating the clean air sources in summer. Although the SOC/OC ratios of PM_{18} in summer and winter were the same, the SOC/OC ratio of $PM_{1.8}$ in winter was particularly higher than that in summer, indicating that photochemical secondary transformation in winter was not the dominant factor to SOC formation in fine particles, while the stable atmosphere and low temperature dominated the formation of SOC.

SOA plays an important role in physical and chemical properties of the atmospheric particles, closely relating to haze, visibility, climate, and health (Reid et al., 2013). The annual average concentration of estimated SOA was 10.88 μg m^{-3}, covering of 11% PM_{18} mass, indicating that SOA also has an important effect on the air pollution in urban Shanghai.

3.3.2. Size distribution of carbonaceous aerosols for different pollution levels

The concentrations of OC, EC and SOC were 4.88, 1.88, 2.33 μg m^{-3} in clean days and 13.14, 5.03, 6.83 μg m^{-3} in polluted days, respectively. The latter increased by 2.69, 2.68 and 2.93 folds than the former, respectively, indicating that the carbonaceous aerosol pollution was very serious in urban Shanghai. The levels of OC, EC and SOC all followed the sequence of coarse mode > condensation mode > droplet mode > nucleation mode in clean days while the sequence changed to condensation mode > droplet mode > condensation mode > nucleation mode in polluted days, implying the unique aerosol formation processes in polluted days. The concentration variations of the size-resolved carbonaceous aerosols in clean and polluted days were presented in Fig. 8. As shown in Fig. 8, the concentration of each carbonaceous species in each mode increased by about 2 fold in polluted cases. The ratio of OC in polluted and clean days followed the sequence of droplet mode > coarse mode > condensation mode > nucleation mode. The contribution of SOC to OC was higher in polluted days than in clean days, and the difference was mainly caused by

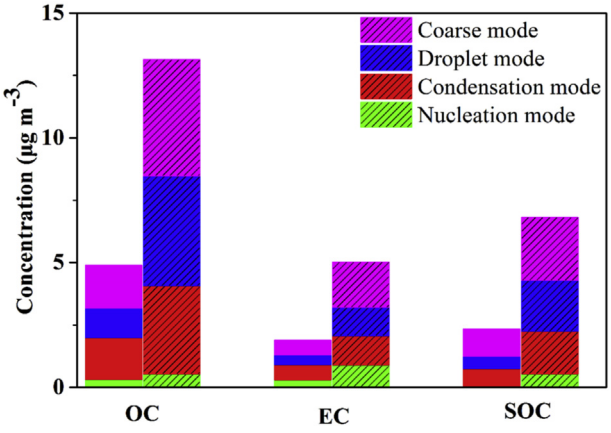

Fig. 8. The concentrations of the size-resolved carbonaceous aerosols in clean and polluted days. Hatched histogram refer to polluted days.

Table 2
Statistical data of size-resolved carbonaceous aerosols in four seasons and in polluted and clean days during the field observation in Shanghai.

Species	Period	Nucleation mode	Condensation mode	Droplet mode	Coarse mode	0.056–18 μm
OC	whole period	0.55	3.69	4.06	4.36	12.66
EC		0.72	1.27	1.04	1.55	4.58
OC/EC		0.76	2.90	3.90	2.81	2.76
SOC		0.50	1.80	1.90	2.58	6.80
SOA		0.80	2.88	3.04	4.13	10.88
SOC/OC	spring	1.00	0.47	0.45	0.68	0.57
	summer	0.37	0.45	0.44	0.62	0.51
	autumn	1.25	0.52	0.49	0.59	0.57
	winter	1.00	0.49	0.47	0.52	0.51

nucleation mode in which OC was totally composed by SOC in polluted days while no SOC was found in nucleation mode in clean days. The values in other modes were close. The highest ratio of the concentration in polluted and clean days for both OC and SOC were in the droplet mode, implying the great contribution of SOC to OC in droplet mode and the occurrence of pollution necessarily had an important bearing on the SOC formation in droplet mode particles.

The OC/EC, SOC/OC in different size modes particles were presented in Table 3. The OC/EC ratios for PM_{18} were almost the same in polluted days and in clean days, it may be explained by the complementary effect of the OC/EC in different size modes, which will be discussed in detail in Section 3.3.3. The maximum OC/EC was in droplet mode and the minimum was in the nucleation mode for both clean and polluted days. The fact that the higher OC, EC, and SOC in polluted days than those in clean days may mean that the air pollution was induced greatly by these species. The higher OC/EC and lower SOC/OC in droplet mode both in polluted days and in clean days may suggest that OC was easy to be concentrated in this mode though SOC was also continuously formed. It should be pointed out that the concentrations of OC and SOC were still lower than that of polluted days though the value in coarse mode in clean days was higher than that in polluted days.

To better understand the change of the carbonaceous aerosols and the particle size distributions of carbonaceous species, the size distribution of particulate matter, OC, EC and SOC under these 5 polluted cases were illustrated in Fig. 9. The log-normal size distributions of OC and EC showed a trimodal with peaks in the particles with size between 0.18 and 0.32 μm, 0.56–1 μm and 5.6–10.0 μm when $PM_{1.8} < 115$ μg m^{-3}. When it comes to heavily and severely polluted cases, OC and EC presented two-peak pattern with one peak in 0.56–1 μm and the other in 5.6–10.0 μm. OC and EC were preferably enriched in fine particles. Mass concentrations of OC and EC in fine particles accounted for 73% and 70% of the total OC and EC. Compared with OC, EC was preferably enriched in particles with size less than 1 μm.

The size distributions of SOC in different polluted cases were not as regular or smooth as those of OC and EC. Weak peaks were found for the size distributions of SOC during clean days while tri-modal and even quad-modal were observed in polluted days, implying the complex formation processes of SOC in the atmosphere. It presented a quad-modal with peaks in the particles with size between 0.18 and 0.32 μm, 0.56–1.0 μm, 1.8–3.2 μm and 5.6–10.0 μm when the atmosphere was lightly or moderately polluted while it was found to be a tri-modal when it was heavily or severely polluted. The peaks for SOC in heavily polluted weathers were 0.1–0.18 μm, 0.32–3.2 μm and 5.6–10 μm. It is noteworthy that during the lightly and moderately polluted days, the size distributions of SOC in atmospheric particles nearly share the peaks with the same size ranges.

The log-normal size distributions of PM shown in Fig. 9 presented a trimodal with peaks in the fine mode (0.56–1 μm) and the coarse mode (5.6–10.0 μm) when $PM_{1.8} < 150$ μg m^{-3}. While the air was severely polluted, the size distribution of atmospheric particles was bimodal but with the main peak moved to a larger size (1–1.8 μm). For the peak of 0.56–1 μm, it might be mainly influenced by OC, EC and the sulfate peak in this size range. As for the peak in 1–1.8 μm in severely polluted days, it might be caused by the combined effect of nitrate, ammonia (see Fig. 5) and SOC. As for the peak in 0.18–0.32 μm, it can be ascribed to SNA. As the main composition that accounted for 18% of the mass concentration, remarkable peak was found for sulfate in the peak size of 0.56–1 μm (Fig. 5), especially in polluted days, thus the contributions of OC and EC (accounting for 10% of PM) to the peak of the PM were weakened. These results may indicate the different size distribution of different composition in PM and may imply the interaction between the formation of SNA, SOC and the formation of mixture state in the atmosphere.

3.3.3. Correlations between OC and EC

3.3.3.1. Correlations between OC and EC in size-resolved particles in different modes. The origins of OC and EC can be assessed by studying the relationship between OC and EC mass concentrations (Turpin and Huntzicker, 1991), for the correlation between OC and EC concentrations should be strong if they were emitted from the similar sources. Typical emission sources of carbonaceous aerosols included diesel- and gasoline-powered vehicle exhaust (OC/EC = 1.0–4.2) (Schauer et al., 2002), fossil fuel combustion (OC/EC = 2.0) (Cao et al., 2006), biomass burning (OC/EC = 9.0) (Cachier et al., 1989), etc. OC/EC ratios were found to be 1.49–4.66 with a mean value of 2.78 for PM_{18} samples and 0.69–9.64 for single size-segregated samples, indicating that vehicle exhaust, fossil fuel combustion and biomass burning were the possible sources of carbonaceous aerosols in urban Shanghai.

EC was usually produced by the incomplete combustion of fossil fuels, biofuel and biomass, which only came from some primary sources, especially from direct vehicle emissions (Zhao et al., 2015). OC level can be disturbed by the primary emission sources from fossil fuel combustion and biofuel/biomass burning, together with secondary formation of SOA. Besides fossil fuel combustion and biofuel burning source emissions, the processes and transport of biomass burning have important contribution to the measured OC. The SOA derived from photochemistry of biogenic or anthropogenic VOCs is an important source of OC. The transport and dispersion of aged aerosol including SOA could also contribute to the OC concentration. Therefore, the relationships between OC and EC concentrations for different size mode particles were analysed (Fig. S2 in the Supplement). Strong correlations were observed between OC and EC for condensation mode (R^2 = 0.85) and droplet mode (R^2 = 0.94) particles, suggesting the same emission sources of combustion and similar transport process for OC and EC in the particles with the size of 0.1–1.8 μm (Zhao et al., 2015). Even so, the high regression slope for droplet mode particles (4.42) indicated that secondary OC in droplet mode particles was likely to be produced by photochemical processes during atmospheric transport while excess primary OC import from different sources may also enhance the value of OC on a transport pathway to urban Shanghai.

Table 3
Statistical data of size-resolved carbonaceous aerosols in polluted and clean days during the field observation in Shanghai.

Species	Period	Nucleation mode	Condensation mode	Droplet mode	Coarse mode	0.056–18 μm
OC	Polluted/Clean	1.95	2.11	3.69	2.69	2.61
EC		3.4	1.94	2.91	2.97	2.81
SOC		/	2.41	4.07	2.26	2.92
OC/EC	Clean	1.08	2.74	3.08	2.79	2.60
	Polluted	0.61	2.96	3.91	2.55	2.61
SOC/OC	Clean	/	0.42	0.42	0.65	0.37
	Polluted	1.00	0.49	0.46	0.55	0.62

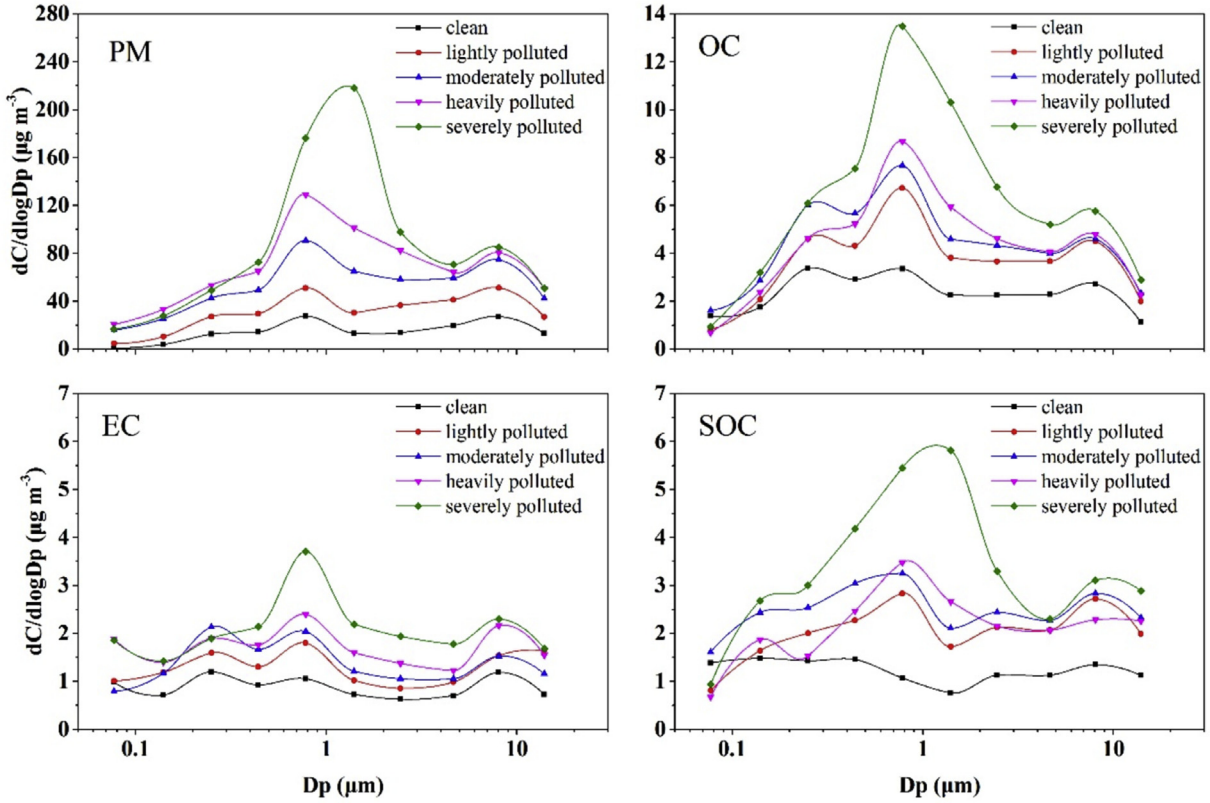

Fig. 9. Size distributions of particulate matter, OC, EC and SOC under 5 pollution conditions (**a**. clear, **b**. lightly polluted, **c**. moderately polluted, **d**. heavily polluted, **e**. severely polluted).

Moreover, OC to EC ratio is commonly regarded as SOA indicator (Chow et al., 1993) and the ratio of 2.2 was assumed to indicate the existence of SOC (Turpin and Huntzicker, 1991). According to this hypothesis, SOA evidently exists in condensation mode and droplet mode, whose OC/EC ratios were 2.94 and 4.42, respectively. The weak correlation between OC and EC for coarse mode ($R^2 = 0.32$) and high OC/EC ratio (2.81) were likely attributed to the influence of different emission sources, the contribution of SOA formation and/or its transport, as well as atmospheric dispersion process of the carbonaceous species in coarse particles in urban Shanghai. No credible relationships between OC and EC were found for nucleation mode particles. This might be accounted to the low carbon loading, the contribution of different source and the secondary formation process in this size range.

3.3.3.2. Correlations between OC and EC in size-resolved particles in four seasons. Table 4 showed the correlations between OC and EC in size-resolved carbonaceous aerosols in four seasons in Shanghai. The least OC/EC ratios were found in particles smaller than 0.056 μm, which were all lower than 1 in four seasons, indicating no secondary reactions for OC. Particles that with the size >0.1 μm all presented with high OC/EC ratios, especially for droplet mode particles, suggesting the enhancement of the secondary formation of OC in the droplet mode. For seasonal comparison, OC/EC ratios were relatively high in cold seasons (winter and spring) versus values in warm seasons (summer and autumn), the reasons might be: (1) more semi-volatile and intermediate-volatile organic compounds adsorbed and condensed into aerosols in lower temperature in cold seasons; (2) more fuel combustion for heating in cold seasons; (3) stable atmosphere, low temperature, low mixing layer height and low precipitation resulted in the accumulation of SOA in winter; (4) lower temperature favours gas-particle equilibrium to move towards the particulate phase; (5) the effect of long-range transport of polluted air with higher OC/EC ratio mainly originated from north and northwest China during cold seasons (Duan et al., 2007).

3.4. Sources of secondary species

3.4.1. PSCF for sulfate, nitrate and SNA in $PM_{1.8}$-associated particles

The concentrations of $PM_{1.8}$-associated SO_4^{2-}, NO_3^- and SNA in Shanghai were 9.44, 2.89 and 11.21 μg m^{-3} in spring, respectively,

Table 4
The ratios of OC/EC in size-resolved carbonaceous aerosols in four seasons during the field observation in Shanghai.

	Seasons	Nucleation mode	Condensation mode	Droplet mode	Coarse mode	PM18	Linear regression equation (single aerosols)	Linear regression equation (daily aerosol samples)
OC/EC	spring	0.72	2.95	3.85	3.70	2.97	OC = 3.36 EC +0.05 (R2 = 0.74)	OC = 4.28 EC - 4.88 ($R^2 = 0.62$)
	summer	0.65	2.49	3.57	3.00	2.5	OC = 3.49 EC - 0.16 (R2 = 0.72)	OC = 2.94 EC - 2.15 ($R^2 = 0.66$)
	autumn	0.79	2.94	3.87	2.46	2.65	OC = 4.08 EC - 0.42 (R2 = 0.74)	/
	winter	0.84	3.07	4.03	2.60	2.84	OC = 3.09 EC - 0.11 (R2 = 0.64)	/

11.01, 0.60 and 11.69 μg m^{-3} in summer, respectively, 7.10, 2.20 and 9.39 μg m^{-3} in autumn, respectively, and 9.82, 10.77 and 20.67 μg m^{-3} in winter, respectively.

Provided daily concentrations of $PM_{1.8}$-associated SO_4^{2-}, NO_3^- and SNA in Shanghai in four seasons, PSCF may provide an effective way to identify the likely locations of atmospheric aerosol sources and show the extent of transport for different species in different seasons. Fig. 10 presented the spatial distributions of the weighted PSCF of $PM_{1.8}$-associated SO_4^{2-}, NO_3^- and SNA in Shanghai in spring, summer, autumn and winter, respectively. It was clearly shown that in addition to local sources, Shanghai was also affected by long-range and meso-scale transport of emissions. In spring and autumn, the daily concentrations of $PM_{1.8}$-associated SO_4^{2-} were relatively lower than those in summer and winter. Potential source areas with weighted PSCF values higher than 0.6 were maily located in the Northern Yellow Sea in spring and the East Japan Sea and some Asian countries such as Japan and Korea in autumn, indicating the role of long-range transported sources to SO_4^{2-} in urban Shanghai in these two seasons. High weighted PSCF values were seen in summer for $PM_{1.8}$-associated SO_4^{2-} in northwest East China Sea (ECS) and the YRD region, indicating that the SO_4^{2-} pollution of Shanghai in summer was mainly ascribed to the influences of sea salt and ship emissions and the inter-regional transport in YRD. However, it was obviously shown in Fig. 10 that the SO_4^{2-} pollution of Shanghai in winter was mainly ascribed to long-range and inter-regional transport and was mainly related to the anthropogenic emissions from inland China.

The daily concentrations of $PM_{1.8}$-associated NO_3^- in spring were similar to those in autumn while they shared the different sources as the NO_3^- in spring had broader potential sources including YRD region and sea sources from the Northern Yellow Sea while the potential sources of $PM_{1.8}$-associated NO_3^- in autumn were mainly ascribed to inter-regional transport. The daily concentrations of $PM_{1.8}$-associated NO_3^- in summer were quite lower than those in other seasons and the criterion, thus the potential sources can not be simulated in this study. Extremely high weighted PSCF values were presented in local Shanghai, the YRD region and northern China, indicating the influence of the considerable amount of anthropogenic pollutants transported from these areas via long-range transport and inter-regional transport on the high loading

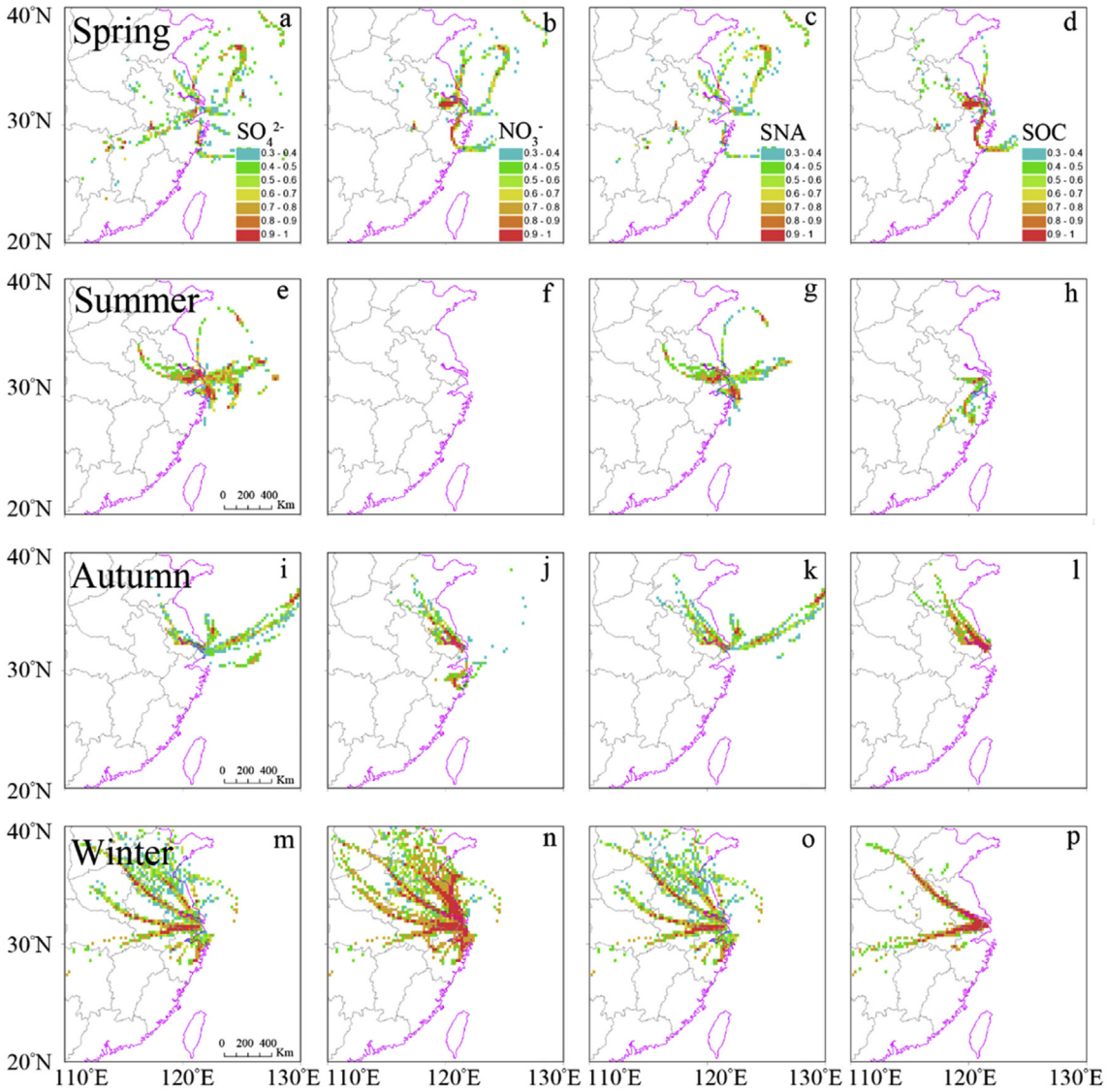

Fig. 10. Spatial distributions of weighted PSCF values for sulfate, nitrate, SNA and SOC in $PM_{1.8}$-associated particles in Shanghai in four seasons (a-p, represent SO_4^{2-}, NO_3^-, SNA and SOC in spring, summer, autumn and winter, respectively).

NO_3^- in winter.

The daily concentrations of $PM_{1.8}$-associated SNA in spring, summer and autumn were quite lower than those in winter. As shown in Fig. 10, the distributions of weighted PSCF values for $PM_{1.8}$-associated SNA in four seasons were almost the combinations of the weighted PSCF for $PM_{1.8}$-associated SO_4^{2-} and NO_3^-, showing the dominant role of SO_4^{2-} and NO_3^- in SNA in this study.

3.4.2. PSCF for SOC in $PM_{1.8}$-associated particles

The concentrations of $PM_{1.8}$-associated SOC in Shanghai were 3.47, 2.11, 4.49 and 6.94 μg m^{-3} in spring, summer, autumn and winter, respectively. Based on the daily concentrations of $PM_{1.8}$-associated SOC in four seasons, weighted PSCF were plotted in Fig. 10. For $PM_{1.8}$-associated SOC, local Shanghai and the neighboring city of Zhejiang and Jiangsu presented high weighted PSCF values in spring, summer and autumn, indicating the contribution of inter-regional transport to the carbonaceous pollution in Shanghai in these seasons. The weighted PSCF results for $PM_{1.8}$-associated SNA in winter identified local Shanghai and the areas that extended from southwest of Shandong province and Hubei province to local Shanghai as the major potential source regions of $PM_{1.8}$-associated SOC in Shanghai in winter, showing the influence of long-range transport on the high loading of carbonaceous pollution in winter in Shanghai.

Compared with the weighted PSCF results of $PM_{1.8}$-associated SO_4^{2-}, NO_3^- and SNA in Shanghai, the potential source regions of SOC in Shanghai shared some similarity with those of inorganic species to some extent. The distributions of weighted PSCF values for $PM_{1.8}$-associated SOC were similar to those for $PM_{1.8}$-associated NO_3^- in spring and winter and the potential source regions of SOC and those of SO_4^{2-}, NO_3^- and SNA in winter belong to the same district, indicating that there may exist some connections between the formation of SOC and the secondary inorganic species in particulate matters.

4. Conclusions

Size-resolved aerosol particle samples were collected with a 10-stage MOUDI at urban Shanghai for four seasons: spring (April 2015), summer (August 2015), autumn (October 2015) and winter (January 2016). Water-soluble ions (i.e., F^-, Cl^-, SO_4^{2-}, NO_3^-, Li^+, Na^+, NH_4^+, K^+, Ca^{2+}, Mg^{2+}, formate, acetate, methanesulfonic acid, oxalate), OC and EC of the atmospheric aerosol particles in the size range of 0.056–18 μm were studied. The particles were divided into four modes: nucleation mode (0–0.1 μm), condensation mode (0.1–0.56 μm), droplet mode (0.56–1.8 μm) and coarse mode (1.8–18 μm). The size distribution of SNA and OC, EC and SOC in four seasons and in different pollution levels were discussed and the potential sources of $PM_{1.8}$-associated secondary species (SO_4^{2-}, NO_3^-, SNA and SOC) in different seasons were identified by PSCF model.

$PM_{1.8}$ ranged from 7.18 to 169.91 μg m^{-3} and averaged 55.32 μg m^{-3}. PM_1 ranged from 5.79 to 95.25 μg m^{-3} and averaged 42.70 μg m^{-3}. $PM_{0.1}$ ranged from 0 to 29.63 μg m^{-3} and averaged 6.03 μg m^{-3}. These results showed that atmospheric ultrafine and fine particle pollution in Shanghai were very serious during the study period. Mass fraction percentage of water-soluble ions in nucleation mode, condensation mode, droplet mode and coarse mode was 19%, 39%, 49% and 24%, respectively. The mass concentrations of the water-soluble ions followed the sequences of $Cl^- > SO_4^{2-} > Ca^{2+} > NO_3^- > Na^+$ for nucleation-mode particles, $SO_4^{2-} > NO_3^- > Na^+ > Cl^- > NH_4^+$ for condensation mode, $SO_4^{2-} > NO_3^- > Na^+ > NH_4^+ > C_2O_4^{2-}$ for droplet mode, and $NO_3^- > SO_4^{2-} > Ca^{2+} > Cl^- > Na^+$ for coarse mode particles, respectively. Most of the water-soluble ions tended to be enriched in fine particles, especially being abundant in the droplet mode in polluted cases. Compared with sulfate, the size distribution of the nitrate and ammonium presented more significant seasonal variations and showed distinctive characteristics in polluted days. Abundant nitrate was concentrated in fine particles in cold seasons (spring and winter), whereas it was enriched in coarse mode during summer and autumn. The droplet mode sulfate with high concentration did not result in the aggravation of air pollution, while the nucleation mode sulfate may have made a great contribution to the air pollution in urban Shanghai. It was also found that the formation of air pollution in urban Shanghai had a significant link with nitrate and ammonium, especially with the nitrate and ammonium in condensation mode and droplet mode, and the contribution of sulfate to the pollution formation in Shanghai would somehow be surpassed by the increasing nitrate and ammonium.

While OC and EC concentrations from spring to winter were 11.10, 7.10, 12.30, 20.16, and 3.73, 2.84, 4.63, 7.10 μg m^{-3}, respectively, distinctly presented the summer minima and winter maxima. SOC concentrations were 6.28, 3.61, 6.95 and 10.36 μg m^{-3} in spring, summer, autumn and winter respectively, accounting for 57%, 51%, 57% and 51% of OC in spring, summer, autumn and winter respectively. Strong correlations were observed between OC and EC for condensation mode ($R^2 = 0.85$) and droplet mode ($R^2 = 0.94$) particles, suggesting the similar emission sources and transport process for carbonaceous aerosols in the particles with the size of 0.1–1.8 μm. The OC/EC ratios were 1.49–4.66 with a mean of 2.78 for PM_{18} samples and 0.69–9.64 for single size-resolved samples, indicating that vehicle exhaust, industrial coal combustion and biomass burning were the possible sources of carbonaceous aerosols in urban Shanghai. The maximum OC/EC was in droplet mode and the minimum was in the nucleation mode for both clean and polluted days. Tri-modal size distributions were found for OC and EC with peaks in the particles with size between 0.18 and 0.32 μm, 0.56–1 μm and 5.6–10.0 μm when $PM_{1.8} < 115$ μg m^{-3} while they presented bi-modal size distributions with peak in 0.56–1 μm and 5.6–10.0 μm when $PM_{1.8} > 115$ μg m^{-3}. The great contribution of SOC to OC in droplet mode and the occurrence of PM pollution necessarily had an important bearing on the SOC formation in droplet mode particles. Particle acidity may play a key role in secondary organic aerosol formation and the particles with the size of 0.056–0.1 μm were the most sensitive particles to acid catalysis in SOA formation. The similar PSCF results of $PM_{1.8}$-associated SOC to those of SO_4^{2-}, NO_3^- and SNA indicated possible connections between the formation of SOC and the secondary inorganic species in PM.

Shanghai has been experiencing severe PM pollution in recent years, and many extensive studies have been conducted to explore the temporal-spatial variations in PM composition and concentrations, sources, formation mechanisms, and evolution processes of PM pollution involving SIA and SOA (Qiao et al., 2015; Wang et al., 2016; Zhao et al., 2015). The enhanced role of SIA and SOA in $PM_{2.5}$ or PM_1 in the formation of haze episode have been revealed (Qiao et al., 2015; Tang et al., 2016). Size distribution characteristics of SIA in size-resolved particles have been investigated (Tao et al., 2014). However, up to now, there is not much research on the size-resolved particles in Shanghai. Results from this study can help to better understand the formation of atmospheric SNA and SOC in different particle modes and their contributions to the occurrence of PM pollution events, and to greatly improve our understanding of the level of air pollution in the Shanghai area.

Conflicts of interest

The authors declare that they have no conflict of interest.

Acknowledgments

This work was supported by National Key R & D Program of China (2017YFC0209505), National Natural Science Foundation of China (Grant Nos. 41475110, 21277028, 21577022 and 21190053) and the Key Project of the Shanghai Municipal Science and Technology Commission (Grant No.14DZ1202903).

Appendix A. Supplementary data

Supplementary data related to this article can be found at http://dx.doi.org/10.1016/j.atmosenv.2017.08.043.

References

Adams, P.J., Seinfeld, J.H., Koch, D.M., 1999. Global concentrations of tropospheric sulfate, nitrate, and ammonium aerosol simulated in a general circulation model. J. Geophys. Res. 104, 13791–13823. http://dx.doi.org/10.1029/1999JD900083.

Andreae, M.O., Schmid, O., Yang, H., Chand, D., Yu, J.Z., Zeng, L.M., Zhang, Y.H., 2008. Optical properties and chemical composition of the atmospheric aerosol in urban Guangzhou, China. Atmos. Environ. 42, 6335–6350. http://dx.doi.org/10.1016/j.atmosenv.2008.01.030.

Arimoto, R., Duce, R.A., Savoie, D.L., Prospero, J.M., Talbot, R., Cullen, J.D., Tomza, U., Lewis, N.F., Ray, B.J., 1996. Relationships among aerosol constituents from Asia and the North Pacific during PEM-West A. J. Geophys. Res. Atmos. 101, 2011–2023. http://dx.doi.org/10.1029/95jd01071.

Ashbaugh, L.L., Malm, W.C., Sadeh, W.Z., 1985. A residence time probability analysis of sulfur concentrations at grand Canyon National Park. Atmos. Environ. 19, 1263–1270. http://dx.doi.org/10.1016/0004-6981(85)90256-2.

Bamber, G., 2012. Source characterization and apportionment of PM_{10}, $PM_{2.5}$ and $PM_{0.1}$ by using positive matrix factorization. Aerosol Air Qual. Res. 12, 476–491. http://dx.doi.org/10.4209/aaqr.2012.04.0084.

Bell, M.L., Davis, D.L., Gouveia, N., Borja-Aburto, V.H., Cifuentes, L.A., 2006. The avoidable health effects of air pollution in three Latin American cities: Santiago, São Paulo, and Mexico City. Environ. Res. 100, 431–440. http://dx.doi.org/10.1016/j.envres.2005.08.002.

Bond, T.C., 2004. A technology-based global inventory of black and organic carbon emissions from combustion. J. Geophys. Res. 109, D14. http://dx.doi.org/10.1029/2003jd003697.

Cachier, H., Brémond, M.P., Buatménard, P., 1989. Carbonaceous aerosols from different tropical biomass burning sources. Nature 340, 371–373. http://dx.doi.org/10.1038/340371a0.

Cao, G., Zhang, X., Zheng, F., 2006. Inventory of black carbon and organic carbon emissions from China. Atmos. Environ. 40, 6516–6527. http://dx.doi.org/10.1016/j.atmosenv.2006.05.070.

Castro, L.M., Pio, C.A., Harrison, R.M., Smith, D.J.T., 1999. Carbonaceous aerosol in urban and rural European atmospheres: estimation of secondary organic carbon concentrations. Atmos. Environ. 33, 2771–2781. http://dx.doi.org/10.1016/s1352-2310(98)00331-8.

Chen, Y., Xie, S.D., 2013. Long-term trends and characteristics of visibility in two megacities in southwest China: Chengdu and Chongqing. J. Air & Waste Manag. Assoc. 63, 1058–1069. http://dx.doi.org/10.1080/10962247.2013.791348.

Chow, J.C., Watson, J.G., Pritchett, L.C., Pierson, W.R., Frazier, C.A., Purcell, R.G., 1993. The dri thermal/optical reflectance carbon analysis system: description, evaluation and applications in U.S. Air quality studies. Atmos. Environ. 27A, 1185–1201. http://dx.doi.org/10.1016/0960-1686(93)90245-T.

Cifuentes, L., Borja-Aburto, V.H., Gouveia, N., Thurston, G., Davis, D.L., 2001. Assessing the health benefits of urban air pollution reductions associated with climate change mitigation (2000-2020): Santiago, São Paulo, México City, and New York City. Environ. Health Perspect. 109 (Suppl 3), 419–425. http://dx.doi.org/10.2307/3434790.

Clegg, S.L., Brimblecombe, P., Wexler, A.S., 1998. A thermodynamic model of H+−NH4+−SO42−NO3−−H2O at tropospheric temperatures. Journal of Physical Chemistry A 102, 2137–2154. http://dx.doi.org/10.1021/jp973042r.

Dibb, J.E., Talbot, R.W., Whitlow, S.I., Shipham, M.C., Winterle, J., Mcconnell, J., Bales, R., 1996. Biomass burning signatures in the atmosphere and snow at Summit, Greenland: An event on 5 August 1994. Atmospheric Environment 30, 553–561. http://dx.doi.org/10.1016/1352-2310(95)00328-2.

Duan, F., Liu, X., Yu, T., Cachier, H., 2004. Identification and estimate of biomass burning contribution to the urban aerosol organic carbon concentrations in Beijing. Atmos. Environ. 38, 1275–1282. http://dx.doi.org/10.1016/j.atmosenv.2003.11.037.

Duan, J., Tan, J., Cheng, D., Bi, X., Deng, W., Sheng, G., Fu, J., Wong, M.H., 2007. Sources and characteristics of carbonaceous aerosol in two largest cities in Pearl River Delta Region, China. Atmos. Environ. 41, 2895–2903. http://dx.doi.org/10.1016/j.atmosenv.2006.12.017.

Dupart, Y., Nekat, B., Nowak, A., Wiedensohler, A., Herrmann, H., David, G., Thomas, B., Miffre, A., Rairoux, P., D'Anna, B., George, C., 2012. Mineral dust photochemistry induces nucleation events in the presence of SO_2. Proc. Natl. Acad. Sci. U. S. A. 109, 20842–20847. http://dx.doi.org/10.1073/pnas.1212297109.

Forster, P.M.D.F., Taylor, K.E., 2006. Climate forcings and climate Sensitivities diagnosed from Coupled climate model integrations. J. Clim. 19, 6181–6194. http://dx.doi.org/10.1175/JCLI3974.1.

Friese, E., Ebel, A., 2010. Temperature dependent thermodynamic model of the system $H^+-NH_4^+-Na^+-SO_4^{2-}-NO_3^--Cl^--H_2O$. J. Phys. Chem. A 114, 11595–11631. http://dx.doi.org/10.1021/jp101041j.

Gao, Y., Lee, S.C., Huang, Y., Chow, J.C., Watson, J.G., 2016. Chemical characterization and source apportionment of size-resolved particles in Hong Kong sub-urban area. Atmos. Res. 170, 112–122. http://dx.doi.org/10.1016/j.atmosres.2015.11.015.

Gray, H.A., Cass, G.R., Huntzicker, J.J., Heyerdahl, E.K., Rau, J.A., 1986. Characteristics of atmospheric organic and elemental carbon particle concentrations in Los Angeles. Environ. Sci. Technol. 20, 580–589. http://dx.doi.org/10.1021/es00148a006.

Guo, H., Sullivan, A.P., Campuzano Jost, P., Schroder, J.C., Lopez Hilfiker, F.D., Dibb, J.E., Jimenez, J.L., Thornton, J.A., Brown, S.S., Nenes, A., 2016. Fine particle pH and the partitioning of nitric acid during winter in the northeastern United States: particle pH and nitric acid partitioning. J. Geophys. Res. Atmos. 121, 10355–10376. http://dx.doi.org/10.1002/2016JD025311.

Han, J.S., Moon, K.J., Lee, S.J., Kim, Y.J., Ryu, S.Y., Cliff, S.S., Yi, S.M., 2005. Size-resolved source apportionment of ambient particles by positive matrix factorization at Gosan background site in East Asia. Atmos. Chem. Phys. 5, 5223–5252. http://dx.doi.org/10.5194/acp-6-211-2006.

He, K., Zhao, Q., Ma, Y., Duan, F., Yang, F., Shi, Z., Chen, G., 2012. Spatial and seasonal variability of PM2.5 acidity at two Chinese megacities: insights into the formation of secondary inorganic aerosols. Atmos. Chem. Phys. 11, 25557–25603. http://dx.doi.org/10.5194/acpd-11-25557-2011.

Hering, S.V., Friedlander, S.K., 1982. Origins of aerosol sulfur size distributions in the Los Angeles basin. Atmos. Environ. 16, 2647–2656. http://dx.doi.org/10.1016/0004-6981(82)90346-8.

Höller, R., Tohno, S., Kasahara, M., Hitzenberger, R., 2002. Long-term characterization of carbonaceous aerosol in Uji, Japan. Atmos. Environ. 36, 1267–1275. http://dx.doi.org/10.1016/S1352-2310(01)00558-1.

Hsu, S.C., Liu, S.C., Huang, Y.T., Chou, C.C.K., Lung, S.C.C., Liu, T.H., Tu, J.Y., Tsai, F., 2009. Long-range southeastward transport of Asian biosmoke pollution: Signature detected by aerosol potassium in Northern Taiwan. J. Geophys. Res. Atmos. 114, 1159–1171. http://dx.doi.org/10.1029/2009JD011725.

Huntzicker, J.J., Johnson, R.L., Shah, J.J., Cary, R.A., 1982. Analysis of Organic and Elemental Carbon in Ambient Aerosols by a Thermal-Optical Method. Springer, US, pp. 79–88.

Iii, C.A.P., Burnett, R.T., Thun, M.J., Calle, E.E., Krewski, D., Ito, K., Thurston, G.D., 2002. Lung Cancer, Cardiopulmonary mortality, and long-term exposure to fine particulate air pollution. Jama J. Am. Med. Assoc. 287, 1132–1141. http://dx.doi.org/10.1001/jama.287.9.1132.

Jang, M., Czoschke, N.M., Lee, S., Kamens, R.M., 2002. Heterogeneous atmospheric aerosol production by acid-catalyzed particle-phase reactions. Science 298, 814–817. http://dx.doi.org/10.1126/science.1075798.

John, W., Wall, S.M., Ondo, J.L., Winklmayr, W., 1990. Modes in the size distributions of atmospheric inorganic aerosol. Atmos. Environ. 24, 2349–2359. http://dx.doi.org/10.1016/0960-1686(90)90327-J.

Laskin, J., Laskin, A., Roach, P.J., Slysz, G.W., Anderson, G.A., Nizkorodov, S.A., Bones, D.L., Nguyen, L.Q., Chem, A., 2010. High-resolution desorption electrospray ionization mass spectrometry for chemical characterization of organic aerosols. Anal. Chem. 82, 2048–2058. http://dx.doi.org/10.1021/ac902801f.

Li, W., Shi, Y., Song, C.L., 2014. Analysis on the Causes and hazards of fog-haze and Prevention Strategies in China. Adv. Mater. Res. 955–959, 3678–3682. 10.4028/www.scientific.net/AMR.955-959.3678.

Li, K., Li, J., Liggio, J., Wang, W., Ge, M., Liu, Q., Guo, Y.C., Tong, S., Li, J., Peng, C., 2017. Enhanced light-scattering of secondary organic aerosols by multiphase reactions. Environ. Sci. Technol. 51, 1285–1292. http://dx.doi.org/10.1021/acs.est.6b03229.

Lin, J.J., Tai, H.S., 2001. Concentrations and distributions of carbonaceous species in ambient particles in Kaohsiung City, Taiwan. Atmos. Environ. 35, 2627–2636. http://dx.doi.org/10.1016/S1352-2310(00)00444-1.

Liu, X.D., Espen, P.V., Adams, F., Cafmeyer, J., Maenhaut, W., 2000. Biomass burning in southern Africa: individual particle characterization of atmospheric aerosols and savanna fire samples. J. Atmos. Chem. 36, 135–155. http://dx.doi.org/10.1023/A:1006387031927.

Liu, C., Liu, Y.C., Ma, J.Z., He, H., 2012. Synergistic reaction between SO_2 and NO_2 on mineral oxides: a potential formation pathway of sulfate aerosol. Phys. Chem. Chem. Phys. 14, 1668–1676. http://dx.doi.org/10.1039/c1cp22217a.

Marple, V.A., Rubow, K.L., Behm, S.M., 1991. A microorifice uniform deposit impactor (MOUDI): description, Calibration, and use. Aerosol Sci. Technol. 14, 434–446. http://dx.doi.org/10.1080/02786829108959504.

Nie, W., Ding, A., Wang, T., Kerminen, V.M., George, C., Xue, L., Wang, W., Zhang, Q., Petäjä, T., Qi, X., 2014. Polluted dust promotes new particle formation and growth. Sci. Rep. 4, 6634. http://dx.doi.org/10.1038/srep06634.

Ondov, J.M., Wexler, A.S., 1998. Where do particulate toxins Reside? An improved Paradigm for the Structure and dynamics of the urban mid-Atlantic aerosol. Environ. Sci. Technol. 32, 2547–2555. http://dx.doi.org/10.1021/es971067y.

Pathak, R.K., Wu, W.S., Wang, T., 2008. Summertime $PM_{2.5}$ ionic species in four major cities of China: nitrate formation in an ammonia-deficient atmosphere. Atmos. Chem. Phys. 9, 1711–1722. http://dx.doi.org/10.5194/acp-9-1711-2009.

Polissar, A.V., Hopke, P.K., Paatero, P., Malm, W.C., Sisler, J.F., 1998. Atmospheric

aerosol over Alaska: 2. Elemental composition and sources. J. Geophys. Res. Atmos. 103, 19045–19057. https://doi.org/10.1029/98JD01212.
Qiao, T., Zhao, M., Xiu, G., Yu, J., 2015. Seasonal variations of water soluble composition (WSOC, Hulis and WSIIs) in PM_1 and its implications on haze pollution in urban Shanghai, China. Atmos. Environ. 123, 306–314. http://dx.doi.org/10.1016/j.atmosenv.2015.03.010.
Reid, J.S., Hyer, E.J., Johnson, R.S., Holben, B.N., Yokelson, R.J., Zhang, J., Campbell, J.R., Christopher, S.A., Di Girolamo, L., Giglio, L., Holz, R.E., Kearney, C., Miettinen, J., Reid, E.A., Turk, F.J., Wang, J., Xian, P., Zhao, G., Balasubramanian, R., Chew, B.N., Janjai, S., Lagrosas, N., Lestari, P., Lin, N.-H., Mahmud, M., Nguyen, A.X., Norris, B., Oanh, N.T.K., Oo, M., Salinas, S.V., Welton, E.J., Liew, S.C., 2013. Observing and understanding the Southeast Asian aerosol system by remote sensing: an initial review and analysis for the Seven Southeast Asian Studies (7SEAS) program. Atmos. Res. 122, 403–468. http://dx.doi.org/10.1016/j.atmosres.2012.06.005.
Schauer, J.J., Kleeman, M.J., Cass, G.R., Simoneit, B.R., 2002. Measurement of emissions from air pollution sources. 4. C1-C27 organic compounds from cooking with seed oils. Environ. Sci. Technol. 36, 567–575. http://dx.doi.org/10.1021/es002053m.
Seinfeld, J.H., Pandis, S.N., 2006. Atmospheric Chemistry and Physics: from Air Pollution to Climate Change, second ed. Wiley, New York.
Sheppard, L., Levy, D., Norris, G., Larson, T.V., Koenig, J.Q., 1999. Effects of ambient air pollution on nonelderly asthma hospital admissions in Seattle, Washington, 1987-1994. Epidemiology 10, 23–30. http://dx.doi.org/10.1097/00001648-199901000-00003.
Squizzato, S., Masiol, M., Agostini, C., Visin, F., Formenton, G., Harrison, R.M., Rampazzo, G., 2016. Factors, origin and sources affecting PM1 concentrations and composition at an urban background site. Atmos. Res. 180, 262–273. http://dx.doi.org/10.1016/j.atmosres.2016.06.002.
Stockwell, W.R., Kuhns, H., Etyemezian, V., Green, M.C., Chow, J.C., Watson, J.G., 2003. The Treasure Valley secondary aerosol study II: modeling of the formation of inorganic secondary aerosols and precursors for southwestern Idaho. Atmos. Environ. 37, 525–534. http://dx.doi.org/10.1016/S1352-2310(02)00895-6.
Strader, R., Lurmann, F., Pandis, S.N., 1999. Evaluation of secondary organic aerosol formation in winter. Atmos. Environ. 33, 4849–4863. http://dx.doi.org/10.1016/S1352-2310(99)00310-6.
Sun, Y., Zhuang, G., Wang, Y., Zhao, X., Li, J., Wang, Z., An, Z., 2005. Chemical composition of dust storms in Beijing and implications for the mixing of mineral aerosol with pollution aerosol on the pathway. J. Geophys. Res. Atmos. 110, 1064–1067. http://dx.doi.org/10.1029/2005JD006054.
Sun, Y.L., Wang, Z.F., Du, W., Zhang, Q., Wang, Q.Q., Fu, P.Q., Pan, X.L., Li, J., Jayne, J., Worsnop, D.R., 2015. Long-term real-time measurements of aerosol particle composition in Beijing, China: seasonal variations, meteorological effects, and source analysis. Atmos. Chem. Phys. 15, 10149–10165. http://dx.doi.org/10.5194/acp-15-10149-2015.
Tang, L., Ding, A., Zhang, Y., Qin, W., Wang, Z., Chen, W., Hua, H., Yang, X., 2016. Regional contribution to PM1 pollution during winter haze in Yangtze River Delta, China. Sci. Total Environ. 541, 161–166. http://dx.doi.org/10.1016/j.scitotenv.2015.05.058.
Tao, Y., Yin, Z., Ye, X., Ma, Z., and Chen, J.: Size distribution of water-soluble inorganic ions in urban aerosols in Shanghai, Atmos. Pollut. Res., 5, 639–647, doi: 10.5094/APR.2014.073, 2014.
Tao, J., Zhang, L., Gao, J., Wang, H., Chai, F., Wang, S., 2015. Aerosol chemical composition and light scattering during a winter season in Beijing. Atmos. Environ. 110, 36–44. http://dx.doi.org/10.1016/j.atmosenv.2015.03.037.
Turpin, B.J., Huntzicker, J.J., 1991. Secondary formation of organic aerosol in the Los Angeles basin: a descriptive analysis of organic and elemental carbon concentrations. Atmos. Environ. Part A General Top. 25, 207–215. http://dx.doi.org/10.1016/0960-1686(91)90291-E.
Turpin, B.J., Huntzicker, J.J., 1995. Identification of secondary organic aerosol episodes and quantitation of primary and secondary organic aerosol concentrations during SCAQS. Atmos. Environ. 29, 3527–3544. http://dx.doi.org/10.1016/1352-2310(94)00276-Q.
Underwood, E., 2017. The polluted brain. Science 355, 342–345. http://dx.doi.org/10.1126/science.355.6323.342.
Wang, Y., Zhuang, G., Sun, Y., An, Z., 2006. The variation of characteristics and formation mechanisms of aerosols in dust, haze, and clear days in Beijing. Atmos. Environ. 40, 6579–6591. http://dx.doi.org/10.1016/j.atmosenv.2006.05.066.
Wang, X., Wang, W., Yang, L., Gao, X., Nie, W., Yu, Y., Xu, P., Zhou, Y., Wang, Z., 2012. The secondary formation of inorganic aerosols in the droplet mode through heterogeneous aqueous reactions under haze conditions. Atmos. Environ. 63, 68–76. http://dx.doi.org/10.1016/j.atmosenv.2012.09.029.
Wang, H.L., Qiao, L.P., Lou, S.R., Zhou, M., Ding, A.J., Huang, H.Y., Chen, J.M., Wang, Q., Tao, S.K., Chen, C.H., 2016. Chemical composition of $PM_{2.5}$ and meteorological impact among three years in urban Shanghai, China. J. Clean. Prod. 112, 1302–1311. http://dx.doi.org/10.1016/j.jclepro.2015.04.099.
Wexler, A.S., Clegg, S.L., 2002. Atmospheric aerosol models for systems including the ions H^+, NH_4^+, Na^+, SO_4^{2-}, NO_3^-, Cl^-, Br^-, and H_2O. J. Geophys. Res. Atmos. 107, 1–14. http://dx.doi.org/10.1029/2001JD000451/asset/jgrd8814.
Whitby, K.T., 1978. The physical characteristics of sulfur aerosols. Atmos. Environ. 12, 135–159. http://dx.doi.org/10.1016/0004-6981(78)90196-8.
Wu, D., Tie, X., Deng, X., 2006. Chemical characterizations of soluble aerosols in southern China. Chemosphere 64, 749–757. http://dx.doi.org/10.1016/j.chemosphere.2005.11.066.
Xiao, H.Y., Liu, C.Q., 2004. Chemical characteristics of water-soluble components in TSP over Guiyang, SW China, 2003. Atmos. Environ. 38, 6297–6306. http://dx.doi.org/10.1016/j.atmosenv.2004.08.033.
Xie, Y., Ding, A., Nie, W., Mao, H., Qi, X., Huang, X., Xu, Z., Kerminen, V.-M., Petäjä, T., Chi, X., Virkkula, A., Boy, M., Xue, L., Guo, J., Sun, J., Yang, X., Kulmala, M., Fu, C., 2015. Enhanced sulfate formation by nitrogen dioxide: implications from in situ observations at the SORPES station. J. Geophys. Res. Atmos. 120, 12,679–12,694. http://dx.doi.org/10.1002/2015JD023607.
Xing, J., Wang, J., Mathur, R., Pleim, J., Wang, S., Hogrefe, C., Gan, C.M., Wong, D., Hao, J., 2016. Unexpected benefits of reducing aerosol cooling effects. Environ. Sci. Technol. 50, 7527–7534. http://dx.doi.org/10.1021/acs.est.6b00767.
Yao, X., Chan, C.K., Fang, M., Cadle, S., Chan, T., Mulawa, P., He, K., Ye, B., 2002. The water-soluble ionic composition of $PM_{2.5}$ in Shanghai and Beijing, China. Atmos. Environ. 36, 4223–4234. http://dx.doi.org/10.1016/S1352-2310(02)00342-4.
Zhang, X.Y., Cao, J.J., Li, L.M., Arimoto, R., Cheng, Y., Huebert, B., Wang, D., 2002. Characterization of atmospheric aerosol over XiAn in the South margin of the loess plateau, China. Atmos. Environ. 36, 4189–4199. http://dx.doi.org/10.1016/S1352-2310(02)00347-3.
Zhang, Q., Jimenez, J.L., Worsnop, D.R., Manjula, C., 2007. A case study of urban particle acidity and its influence on secondary organic aerosol. Environ. Sci. Technol. 41, 3213–3219. http://dx.doi.org/10.1021/es061812j.
Zhao, B., Wang, S., Dong, X., Wang, J., Duan, L., Fu, X., Hao, J., Fu, J., 2013. Environmental effects of the recent emission changes in China: implications for particulate matter pollution and soil acidification. Environ. Res. Lett. 8, 279–288. http://dx.doi.org/10.1088/1748-9326/8/2/024031.
Zhao, M., Huang, Z., Qiao, T., Zhang, Y., Xiu, G., Yu, J., 2015. Chemical characterization, the transport pathways and potential sources of $PM_{2.5}$ in Shanghai: seasonal variations. Atmos. Res. 158, 66–78. http://dx.doi.org/10.1016/j.atmosres.2015.02.003.
Zhou, S., Wang, Z., Gao, R., Xue, L., Yuan, C., Wang, T., Gao, X., Wang, X., Nie, W., Xu, Z., Zhang, Q., Wang, W., 2012. Formation of secondary organic carbon and long-range transport of carbonaceous aerosols at Mount Heng in South China. Atmos. Environ. 63, 203–212. http://dx.doi.org/10.1016/j.atmosenv.2012.09.021.